AĞRI
İBRAHİM ÇEÇEN
UNIVERSITY
2007

EASTERN ANATOLIAN JOURNAL OF SCIENCE
2015

$\pi = 3,14159\%$

Owner on Behalf of Ağrı İbrahim Çeçen University

Prof. Dr. Abdulhalik KARABULUT

Rector

Editor-in-Chief

Prof. Dr. İbrahim HAN

ihan@agri.edu.tr

Associate Editor

Assoc. Prof. Dr. Abdullah ÇAĞMAN

acagman@agri.edu.tr

PREFACE

Dear scientist,

I am happy to announce that Volume IX - Issue I of the Eastern Anatolian Journal of Science (EAJS) has been published. This issue is composed of 5 research articles that possess some of the leading and advanced techniques of natural and applied sciences. On behalf of the owner of EAJS, I would like to thank all authors, referees, our editorial board members and section editors that provide valuable contributions for the publication of the issue.

EAJS will publish original and high-quality articles covering a wide range of topics in scientific research, dedicated to promoting high standards and excellence in the creation and dissemination of scientific knowledge. EAJS published in English is open access journal and abstracting and indexing by various international index services.

Authors are solicited to contribute to the EAJS by submitting articles that illustrate research results, projects, surveying works and industrial experiences that describe significant advances in the following areas, but are not limited to:

- ➢ Biology
- ➢ Chemistry
- ➢ Engineering
- ➢ Mathematics
- ➢ Nanoscience and Nanotechnology
- ➢ Physics

Our previous issues have an attraction in terms of scientific quality and impact factor of articles by favorable feedbacks of readers. Our editorial team lend wings to be an internationally reputable and pioneer journal of science by their outstanding scientific personality. I am hoping to work effectively with our editorial team in the future.

I'd like to express my gratitude to all authors, members of editorial board and contributing reviewers. My sincere thanks go to Prof. Dr. Abdulhalik KARABULUT, the rector of Ağrı İbrahim Çeçen University, sets the goal of being also a top-ranking university in scientific sense, for supporting and motivating us in every respect. I express my gratitude to the members of technical staff of the journal for the design and proofreading of the articles. Last but not least, my special thanks go to the respectable businessman Mr. İbrahim ÇEÇEN who unsparingly supports our university financially and emotionally, to his team and to the director and staff of IC foundation.

I invite scientists from all branches of science to contribute our journal by sending papers for publication in EAJS.

Prof. Dr. İbrahim HAN

Editor-in-Chief

CONTENTS

The Fekete-Szegö problem for certain subclass of analytic and univalent functions associated with hyperbolic sine function with the complex order

Nizami MUSTAFA [1], Veysel NEZİR [2] and Arzu KANKILIÇ [3*]

[1] *Kafkas University, Faculty of Science and Letters, Department of Mathematics, Kars, Turkiye,*
nizammstafa@gmail.com (ORCID:0000-0002-2758-0274)

[2] *Kafkas University, Faculty of Science and Letters, Department of Mathematics, Kars, Turkiye,*
veyselnezir@yahoo.com (ORCID:0000-0001-9640-8526)

[*3] *Kafkas University, Faculty of Science and Letters, Department of Mathematics, Kars, Turkiye,*
arzucalimgil@gmail.com (ORCID: 0009-0009-4543-9918)

Abstract

In this paper, we give coefficient estimates for the certain subclass of analytic and univalent functions on the open unit disk in the complex plane associated with hyperbolic sine function with the complex order. For the subclass $C_{\sinh}(\tau)$, $\tau \in \mathbb{C} - \{0\}$ defined here of analytic and univalent functions, with the quantity

$$1 + \frac{1}{\tau}\left[\frac{(zf'(z))'}{f'(z)} - 1\right]$$

subordinated to $1 + \sinh z$, we obtain coefficient estimates for initial two coefficients and examine the Fekete-Szegö problem.

1. Introduction

The main focus of this section is to give some basic information that we will use in the proof of the main results.

Let $H(U)$ be the class of all analytic functions in $U = \{z \in \mathbb{C}: |z| < 1|\}$. By A, we will denote the class of functions $f \in H(U)$ given by the following series expansion, explicitly satisfying the conditions $f(0) = 0$ and $f'(0) - 1 = 0$

$$f(z) = z + a_2 z^2 + a_3 z^3 + \cdots$$
$$= z + \sum_{n=2}^{\infty} a_n z^n, a_n \in \mathbb{C}. \qquad (1.1)$$

Moreover, let S be a subclass of all univalent functions of A. The class S was first time introduced by Köebe (Köebe 1909) and has become a core component of research in this area. Bieberbach (Bieberbach 1916) published a paper in which the famous coefficient hypothesis was proposed. This conjecture states that if $f \in S$ and has the series form (1.1), then $|a_n| \le n$ for all $n \ge 2$. Many mathematicians worked hard to solve this problem. But for the first time in 1985 it was De-Branges (De-Branges 1985) who settled this long-lasting conjecture.

It is well-know that a univalent function $f \in S$ is called a convex function, if this function maps open unit disk U onto the convex shaped domain of the complex plane. The set of all convex functions which satisfies the following condition is denoted by C

$$\mathrm{Re}\left(\frac{(zf'(z))'}{f'(z)}\right) > 0, \ z \in U \ ;$$

that is,

$$C = \left\{ f \in S: \ \mathrm{Re}\left(\frac{(zf'(z))'}{f'(z)}\right) > 0, \ z \in U \right\}.$$

Some of the important and well-investigated subclass of S include the class $C(\alpha)$ given below, which called the class of convex functions of order $\alpha \ (\alpha \in [0,1))$

$$C(\alpha) = \left\{ f \in S: \ \mathrm{Re}\left(\frac{(zf'(z))'}{f'(z)}\right) > \alpha, \ z \in U \right\}.$$

2. Materials and Methods

It is well-known that an analytical function ω satisfying the conditions $\omega(0) = 0$ and $|\omega(z)| < 1$ is called Schwartz function. Two analytic functions f and g in U are said that f is subordinate to g and denoted by $f \prec g$, if there exists a Schwartz function ω, such that $f(z) = g(\omega(z))$.

In 1994, Ma and Minda (Ma and Minda 1994) using subordination terminology was defined the class $C(\varphi)$ as follows

$$C(\varphi) = \left\{ f \in S : \frac{(zf'(z))'}{f'(z)} \prec \varphi(z), z \in U \right\},$$

where $\varphi(z)$ is a univalent function with $\varphi(0) = 1$, $\varphi'(0) > 0$ and the region $\varphi(U)$ is star-shaped about the point $\varphi(0) = 1$ and symmetric with respect to real axis. Such a function has a series expansion of the following form

$$\varphi(z) = 1 + b_1 z + b_2 z^2 + b_3 z^3 + \cdots$$
$$= 1 + \sum_{n=1}^{\infty} b_n z^n, \ b_1 > 0 .$$

In the past few years, numerous subclasses of the collection S have been introduced as special choices of the function φ (see for example (Sokol 2011, Janowski 1970, Arif, et al 2019, Brannan 1969, Sokol and Stankiewcz et al. 2021, Sharma et al. 2016, Kumar and Arora 2020, Mendiratta et a.l 2015, Shi et al 2019, Bano and Raza 2020, Alotaibi et al. 2020, Ullah et al. 2021, Cho et al. 2019, Mustafa et al.2022, Mustafa 2017, Xu et al, 2012)).

Finding bounds for the function coefficients in a given collection is one of the most fundamental problems in geometric function theory.

As known that the first order of Hankel determinant of the function $f \in S$ defined as follows

$$H_{2,1}(f) = \begin{vmatrix} 1 & a_2 \\ a_2 & a_3 \end{vmatrix} = a_3 - a_2^2 .$$

The functional $H_{2,1}(f, \mu) = a_3 - \mu a_2^2$ is known as the generalized Fekete-Szegö functional, where μ is a complex or real number (Duren 1983). Estimating the upper bound of $|a_3 - \mu a_2^2|$ is known as the Fekete-Szegö problem in the theory of analytic functions.

Now by using the definition of subordination, we introduce a new subclass of analytic and univalent functions associated with sine hyperbolic function as follows.

Definition 2.1. For $\tau \in \mathbb{C} - \{0\}$ a function $f \in S$ is said to be in the class $C_{\sinh}(\tau)$, if the following condition is satisfied

$$1 + \frac{1}{\tau}\left[\frac{(zf'(z))'}{f'(z)} - 1 \right] \prec 1 + \sinh z, z \in U ;$$

that is,

$$C_{\sinh}(\tau) \equiv C(\tau, 1 + \sinh z)$$
$$= \left\{ f \in S : \frac{(zf'(z))'}{f'(z)} \prec 1 + \sinh z \right\}, \ z \in U.$$

Remark 2.1. In the cases $\tau = 1$, we have class $C_{\sinh} \equiv C(1 + \sinh z)$ which reviewed in (Mustafa et al. 2023).

Let P be the class of analytic functions in U satisfied the conditions $p(0) = 1$ and $\text{Re}(p(z)) > 0$, $z \in U$, which from the subordination principle easily can written

$$P = \left\{ p \in A : p(z) \prec \frac{1+z}{1-z}, z \in U \right\},$$

where $p(z)$ has the series expansion of the form

The Fekete-Szegö problem for certain subclass of analytic and univalent functions
associated with hyperbolic sine function with the complex order

EAJS, Vol. 9 Issue 1 | **3**

$$p(z) = 1 + p_1 z + p_2 z^2 + p_3 z^3 + \cdots$$

$$= 1 + \sum_{n=1}^{\infty} p_n z^n, \ z \in U \ . \tag{2.1}$$

The class P defined above is known as the class Caratheodory functions (Miller 1975).

Let's present some necessary lemmas known in the literature for the proof of our main results.

Lemma 2.1. (Duren 1983). Let the function $p(z)$ belong in the class P. Then,

$|p_n| \leq 2$ for each $n \in \mathbb{N}$ and $|p_n - \lambda p_k p_{n-k}| \leq 2$

for $n, k \in \mathbb{N}, n > k$ and $\lambda \in [0,1]$.

The equalities hold for

$$p(z) = \frac{1+z}{1-z} \ .$$

Lemma 2.2. (Duren 1983) Let the analytic function $p(z)$ be of the form (1.2), then

$$2 p_2 = p_1^2 + \left(4 - p_1^2\right) x ,$$

$$4 p_3 = p_1^3 + 2\left(4 - p_1^2\right) p_1 x - \left(4 - p_1^2\right) p_1 x^2$$

$$+ 2\left(4 - p_1^2\right)\left(1 - |x|^2\right) y$$

for $x, y \in \square$ with $|x| \leq 1$ and $|y| \leq 1$.

3. Results

In this section, we give upper bound estimates for initial two coefficients for the function class $C_{\text{sinh}}(\tau)$ and examine Fekete-Szegö problem for this class.

Let us first give the following theorem.

Theorem 3.1. Let the function $f \in A$ given by (1.1) belong to the class $C_{\text{sinh}}(\tau)$. Then,

$$|a_2| \leq \frac{|\tau|}{2}$$

and

$$|a_3| \leq \frac{|\tau|}{6} \begin{cases} 1 & \text{if} \quad |\tau| \leq 1, \\ |\tau| & \text{if} \quad |\tau| \geq 1. \end{cases}$$

Proof. Let $f \in C_{\text{sinh}}(\tau)$. Then, there exists a Schwartz function $\omega(z)$, such that

$$\frac{\left(z f'(z)\right)'}{f'(z)} = 1 + \tau \cdot \sinh \omega(z), \ z \in U \ .$$

By writing the Caratheodory function $p \in P$ in terms of Schwartz function ω, we have

$$p(z) = \frac{1 + \omega(z)}{1 - \omega(z)} = 1 + p_1 z + p_2 z^2 + \cdots \ .$$

It follows from that

$$\omega(z) = \frac{p(z) - 1}{p(z) + 1}$$

$$= \frac{1}{2} p_1 z + \frac{1}{2}\left(p_2 - \frac{p_1^2}{2}\right) z^2 + \cdots \ . \tag{3.1}$$

From the series expansion (1.1) of the function $f(z)$, we can write

$$\frac{\left(z f'(z)\right)'}{f'(z)} = 1 + 2 a_2 z + 2\left(3 a_3 - 2 a_2^2\right) z^2 + \cdots \ . \tag{3.2}$$

Since

$$\sinh z = z + \frac{1}{3!} z^3 + \frac{1}{5!} z^5 + \cdots , \tag{3.3}$$

from the series expansion (3.1) of the function $\omega(z)$, we have

$$1 + \tau \cdot \sinh \omega(z)$$

$$= 1 + \frac{\tau}{2} p_1 z + \frac{\tau}{2}\left(p_2 - \frac{p_1^2}{2}\right) z^2 + \cdots \ . \tag{3.4}$$

Equalizing (3.2) and (3.4), then comparing the coefficients of the same degree terms on the right and left sides, we obtain the following equalities for two initial coefficients of the function $f(z)$

$$a_2 = \frac{\tau}{4} p_1, \qquad (3.5)$$

$$a_3 = \frac{\tau(\tau-1)}{24} p_1^2 + \frac{\tau}{12} p_2. \qquad (3.6)$$

Using Lemma 2.1, from the equalities (3.5) we can easily see that

$$|a_2| \le \frac{|\tau|}{2}.$$

Applying the Lemma 2.2, the equality (3.6) we can write as follows

$$a_3 = \frac{\tau}{24}\left(\tau p_1^2 + \left(4 - p_1^2\right)x\right), \qquad (3.7)$$

where $x \in \square$ with $|x| \le 1$. Applying triangle inequality, from this equality to (3.7) we obtain

$$|a_3| \le \frac{|\tau|}{24}\left(|\tau|t^2 + \left(4 - t^2\right)\xi\right),$$

where $\xi = |x|$ and $t = |p_1|$. If we maximize the function $\varphi: [0,1] \to \mathbb{R}$ defined as follows

$$\varphi(\xi) = |\tau|t^2 + \left(4 - t^2\right)\xi, \ \xi \in [0,1],$$

we write

$$|a_3| \le \frac{|\tau|}{24}\left((|\tau|-1)t^2 + 4\right), \ t \in [0,2].$$

From this, we obtain desired estimate for $|a_3|$.

Thus, the proof of the theorem is completed.

Taking $\tau = 1$ in Theorem 3.1, we obtain the following result for $|a_2|$ and $|a_3|$ obtained in (Mustafa et al. 2023).

Theorem 3.2. Let the function $f \in A$ given by (1.1) belong to the class C_{sinh}.
Then, we have

$$|a_2| \le \frac{1}{2} \text{ and } |a_3| \le \frac{1}{6}.$$

Let us now give the following theorem on the Fekete-Szegö inequality.

Theorem 3.3. Let the function $f \in A$ given by (1.1) belong to the class $C_{\text{sinh}}(\tau)$ and $\mu \in \mathbb{C}$. Then,

$$\left|a_3 - \mu a_2^2\right| \le \frac{|\tau|}{6}\begin{cases} 1 & \text{if } |2-3\mu||\tau| \le 2, \\ \dfrac{|2-3\mu||\tau|}{2} & \text{if } |2-3\mu||\tau| \ge 2. \end{cases}$$

Proof. Let $f \in C_{\text{sinh}}(\tau)$ and $\mu \in \mathbb{C}$. From the equalities (3.5) and (3.6), using Lemma 2.2 we can write

$$a_3 - \mu a_2^2 = \frac{\tau}{16}\left[\left(\frac{2}{3} - \mu\right)\tau p_1^2 + \frac{2}{3}\left(4 - p_1^2\right)x\right], \qquad (3.8)$$

where $x \in \square$ with $|x| \le 1$. From this equality, applying triangle inequality we can write

$$\left|a_3 - \mu a_2^2\right| \le \frac{|\tau|}{16}\left[\left|\frac{2}{3} - \mu\right||\tau|t^2 + \frac{2}{3}\left(4 - t^2\right)\xi\right],$$
$$\xi \in [0,1] \qquad (3.9)$$

with $t = |p_1| \in [0,2]$ and $\xi = |x|$.

By maximizing the function

$$\psi(\xi) = \left|\frac{2}{3} - \mu\right||\tau|t^2 + \frac{2}{3}\left(4 - t^2\right)\xi, \ \xi \in [0,1],$$

from the inequality (3.9), we obtain the following inequality

$$\left|a_3 - \mu a_2^2\right| \le \frac{|\tau|}{16}\left\{\left[\left|\frac{2}{3} - \mu\right||\tau| - \frac{2}{3}\right]t^2 + \frac{8}{3}\right\},$$
$$t \in [0,2]. \qquad (3.10)$$

The Fekete-Szegö problem for certain subclass of analytic and univalent functions
associated with hyperbolic sine function with the complex order

EAJS, Vol. 9 Issue 1 | 5

From here, we obtained the desired result of the theorem.

Thus, the proof of theorem is completed.

Taking $\tau = 1$ in Theorem 3.3, we obtain the following result for the Fekete-Szegö inequality obtained in (Mustafa et al. 2023).

Theorem 3.4 . Let the function $f \in A$ given by (1.1) belong to the class $C_{\sinh}$ and $\mu \in \mathbb{C}$. Then,

$$\left| a_3 - \mu a_2^2 \right| \leq \frac{1}{6} \begin{cases} 1 & \text{if } |2-3\mu| \leq 2, \\ \dfrac{|2-3\mu|}{2} & \text{if } |2-3\mu| \geq 2. \end{cases}$$

In case $\mu \in \mathbb{R}$, Theorem 3.3 is given as below.

Theorem 3.5. Let the function $f \in A$ given by (1.1) belong to the class $C_{\sinh}(\tau)$ and $\mu \in \mathbb{R}$. Then,

$$\left| a_3 - \mu a_2^2 \right|$$

$$\leq \frac{|\tau|}{6} \begin{cases} 1 & \text{if } \mu \in \left[\dfrac{2(|\tau|-1)}{3|\tau|}, \dfrac{2(|\tau|+1)}{3|\tau|} \right], \\ \dfrac{|2-3\mu||\tau|}{2} & \text{if } \mu \leq \dfrac{2(|\tau|-1)}{3|\tau|} \text{ or } \mu \geq \dfrac{2(|\tau|+1)}{3|\tau|}. \end{cases}$$

The proof of this theorem is done similarly to the proof of Theorem 3.3.

Taking $\mu = 0$ and $\mu = 1$ in Theorem 3.5, we get the estimate for $|a_3|$ obtained in Theorem 3.1 and the following result, respectively.

Corollary 3.1. If the function $f \in A$ given by (1.1) belong to the class $C_{\sinh}(\tau)$, then

$$\left| a_3 - a_2^2 \right| \leq \frac{|\tau|}{6} \begin{cases} 1 & \text{if } |\tau| \leq 2, \\ \dfrac{|\tau|}{2} & \text{if } |\tau| \geq 2. \end{cases}$$

Taking $\tau = 1$ in Corollary 3.1, we obtain the following result obtained in (Mustafa et al. 2023).

Corollary 3.2. If the function $f \in A$ given by (1.1) belong to the class $C_{\sinh}$, then

$$\left| a_3 - a_2^2 \right| \leq \frac{1}{6}.$$

4. Discussion

In this study, we obtained the results obtained in (Mustafa et al. 2023) for wider function classes.

Really, it can be easily seen the results in (Mustafa et al. 2023) are obtained if we take $\tau = 1$ in our study.

References

ARMSTRONG, B., THÉRIAULT, G., GUÉNEL, P., DEADMAN, J., GOLDBERG, M., HÉROUX, P. (1994). Association between exposure to pulsed electromagnetic fields and cancer in electric utility workers in Quebec, Canada, and France. *Am J Epidemiol 1994*, 140:805-820.

ALOTAİBİ, A., ARİF, M., ALGHAMDİ, M. A., HUSSAİN, S. (2020) Starlikness associated with cosine hyperbolic function. *Mathematics*. 8(7), p. 1118.

ARİF, M., AHMAD, K., LİU, J.-L., SOKOL, J. (2019). A new class of analytic functions associated with Salagean operatör. *Hindawi Journal of Function Spaces*. Article ID 6157394, 8 pages https://doi.org/10.1155/2019/6157394

BANO, K., RAZA, M. (2020) Starlike functions associated with cosine function. *Bull. Iran. Math. Soc*. 47: pp. 1513-1532.

BİEBERBACH, L. (1916) Uber die Koeffizienten derjenigen Potenzreihen, welche eine schlichte Abbildung des Einheitskreises vermitteln. *Sitzungsberichte Preuss. Akad. Der Wiss.* 138: pp. 940-955

BRANNAN, D. A., KİRWAN, W. E. (1969) On some classes of bounded univalent functions. *J. Lond. Math*. Soc. 2: pp. 431-443.

CHO, N. E., KUMAR, V., KUMAR, S. S., RAVİCHANDRAN, V. (2019) Radius problems for starlike functions associated with the sine function. Bull. Iran. Math. Soc. 45: pp. 213-232.

DE BRANGES, L. (1985) A proof of the Bieberbach conjecture. Acta Math. 154: pp. 137-152.

DUREN, P. L. (1983) Univalent Functions. In Grundlehren der Mathematischen Wissenschaften, New York, Berlin, Heidelberg and Tokyo, *Springer-Verlag,* Volume 259.

JANOWSKİ, W. (1970) Extremal problems for a family of functions with positive real part and for some related families. Ann. Pol. Math. 23: pp. 159-177.

KÖEBE, P. (1909) Über die Uniformisierrung der algebraishen Kurven, durch automorpher Funktionen mit imaginarer *Substitutionsgruppe. Nachr. Akad. Wiss. Göttingen Math.-Phys*. pp. 68-76.

KUMAR, S. S., ARORA, K. (2020) Starlike functions associated with a petal shaped domain. *ArŞi*v: 2010.10072

MA, W. C., MİNDA, D. (1994) A unified treatment of some special classes of univalent functions. In Proceedings of the Conference on Complex Analysis, Tianjin, China, Li, Z., Ren, F., Yang, L., Zhang, S., Eds.; *Conference Proceedings and Lecture Notes in Analysis; Internotianal Press: Cambridge, MA, USA*, Volume 1, pp. 157-169.

MENDİRATTA, R., NAGPAL, S., RAVİCHANRAN, V. (2015) On a subclass of strongly starlike functions assiociated with exponential function. *Bull. Malays. Math. Soc*. 38, pp. 365-386.

MİLLER, S. S. (1975) Differential inequalities and Caratheodory functions. *Bull. Am. Math. Soc*. 1975, 81, pp. 79-81.

MUSTAFA N. KORKMAZ S. (2022) Coefficient Bound Estimates and Fekete-Szegö Problemfor a Certain Subclass of Analytic and Bi-univalent Functions. T*urkish Journal of Science*. 7(3), 211-218.

MUSTAFA N. (2017) Fekete-Szegö Problem for certain subclass of analytic and bi-univalent functions. *Journal of Scientific and Engineering Research*. 4(8), 30–40.

MUSTAFA, N., NEZİR, V., KANKILIÇ. A. (2023) The Fekete-Szegö problem for certain subclass of analytic and univalent functions associted with sine hyperbolic function. *13th International Istanbul Scientific Research Congress on Life, Engineering and Applied Sciences on April* 29-30: pp. 242-249, Istanbul, Turkey.

SHARMA, K., JAİN, N. K., RAVİCHANRAN, V. (2016) Starlike function associated witha cardioid. Afr. Math. 27: pp. 923-939.

SHİ,. L., SRİVASTAVA, H. M. ARİF, M., HUSSAİN, S., KHAN, H. (2019) An investigation of the third Hankel determinant problem for certain subfamilies of univalent functions involving the exponential function. Symmetry. 11: p.598.

SOKOL, J. (2011). A certain class of starlike functions. *Comput. Math. Appl*. 62, pp. 611-619.

SOKOL, J., STANKİEWCZ, J. (2021). Radius of conexity of some subclasses of strongy starlike functions. Zesyty Nauk. *Bull. Sci. Math*., 167, 102942.

ULLAH, K., ZAİNAB, S., ARİF, M., DARUS, M., SHUTAYİ, M. (2021) Radius Problems for Starlike Functions Associated with the Tan Hyperbolic Function. *Hindawi Journal of Function Spaces Volume 202*, Article ID 9967640, 15 pages https://doi.org/10.1155/2021/9967640 .

XU QH, XİAO G, SRİVASTAVA H.M. (2012) A certain general subclass of analytic and bi-univalent functions and associated coefficient estimate problems. *Applied Mathematics and Computation.* 218, 11461–11465.

A Computational Study on Radiation Shielding Potentials of Eutectic High Entropy Alloys

Zeynep AYGUN[*1], Murat AYGUN[2]

[*1]*Bitlis Eren University, Vocational School of Technical Sciences, 13100, Bitlis, Turkiye*
zeynep.yarbasi@gmail.com (ORCID: 0000-0002-2979-0283)
[2]*Bitlis Eren University, Faculty of Science and Arts, Department of Physics, 13100, Bitlis, Turkiye*
maygun@beu.edu.tr (ORCID: 0000-0002-4276-3511)

Abstract

Eutectic high entropy alloy, a new kind of high entropy alloy, has great interest due to the widespread use in high temperature applications with perfect mechanical features. Our motivation to do this work is the absence of studies about the radiation shielding performances of this new type alloys. The aim of the work was to determine the photon protection parameters such as linear and mass attenuation coefficients, mean free path, half value layer, effective atomic number, fast neutron removal cross section and buildup factors of the eutectic high entropy alloys, ($CoCrFeNiNb_{0.25}Ta_{0.20}$; $CoCrFeNiTa_{0.4}$;$CoCrFeNiTa_{0.75}$;$CoCrFeNiTa_{0.25}Hf_{0.25}$; $Co_2Mo_xNi_2VW_x$) by using Phy-X/PSD software. XCom was also performed to obtain the mass attenuation coefficients of the alloys, and a good agreement was obtained. It was concluded that $Co_2Mo_xNi_2VW_x$ has the most shielding property while $CoCrFeNiNb_{0.25}Ta_{0.20}$ shows the least shielding feature among the alloys. It was also determined that $Co_2Mo_xNi_2VW_x$ has the highest neutron shielding ability. As a result, it is noted that eutectic high entropy alloys can be evaluated as new type shielding materials for radiation related applications.

Keywords: Photon protection parameters, EHEAs, Phy-X/PSD.

1. Introduction

Since reported firstly by Cantor et al. (2004) and Yeh et al. (2004), high entropy alloys (HEAs) are the new alloy systems consisting of at least four major elements. HEAs with perfect mechanical, thermal and chemical properties have great interest from researchers (Aygun 2023; Sakar et al. 2023; Chen et al. 2023; Xiao et al. 2020). Recently, eutectic HEAs (EHEAs) have been proposed as a kind of HEAs firstly by Lu et al. (2014) by adding an appropriate element to the HEA. The combination of FCC (ductile phase) with BCC or intermetallic ones (hard phase) with good creep resistance and stable defect structures makes the alloys attractive for the studies in high temperature applications. The microstructure features of the EHEAs are also effective for radiation resistance in materials (Wang et al. 2023). EHEAs can be used in several industries, such as aerospace, automotive, electronics, etc. Therefore, recently, many researches have been carried out by developing eutectic microstructures for the purpose of obtaining better combination of mechanical properties (Wang et al. 2023; Jiao et al. 2023; Mukarram et al. 2021; Li et al. 2022; Chen et al. 2021).

Increasing application areas of radiation and technological developments necessitate the production of effective radiation shielding materials for human health. The alloys used in high temperature and radiation related applications were studied for their radiation shielding performances previously (Xiao et al. 2020; Chen at al. 2023; Sakar et al. 2023; Aygun, 2023; Aygun and Aygun, 2023). But, the new type EHEAs have not been studied by radiation protection features, yet. The objective of determining radiation shielding properties of the EHEAs is necessary for closing this lack in the literature. The linear and mass attenuation coefficients (LAC and MAC), effective atomic number (Z_{eff}), mean free path

(MFP), half value layer (HVL), atomic cross section (ACS), electronic cross section (ECS), fast neutron removal cross section (FNRCS) and build up factors (EBF and EABF) are the photon protection parameters which are significant to learn the degree of protection of the alloys. In this regard, for the purpose of estimating the photon protection performances of the alloys (CoCrFeNiNb0.25Ta0.20/D1; CoCrFeNiTa0.4/D2; CoCrFeNiTa0.75/D3; CoCrFeNiTa0.25Hf0.25/D4; Co2MoxNi2VWx/D5) Phy-X/PSD developed for shielding, photon attenuation and dosimetry including a wide energy range of 1 keV-100 GeV was used. XCom software (Berger and Hubbell, 1987) was also used which is developed to acquire photon interaction cross-sections and MAC values of an element, compound or mixture in the 1 keV–100 GeV wide energy region.

2. Materials and Methods

In the study, EHEAs reported previously for their mechanical properties were chosen. The chemical components of the alloys were used for the calculations (Jiang et al. 2016; Jiang et al. 2018; Mukarram et al. 2021; Jiao et al. 2023) and given in Table 1.

The rule of mixture is used for calculation of density (ρ_{mix}) of the alloys (Xiang et al. 2019):

$$\rho_{mix} = \frac{\sum_{i=1}^{n} c_i A_i}{\frac{\sum_{i=1}^{n} c_i A_i}{\rho_i}} \tag{1}$$

A_i, c_i and ρ_i, and are atomic fraction, atomic weight of element i_{th} and density, respectively.

The MAC can be found by the Eq. 2:

$$I = I_0 e^{-\mu t} \tag{2}$$

$$\mu_m = \frac{\mu}{\rho} = ln(I_0/I)/\rho t = ln(I_0/I)/t_m \tag{3}$$

where μ (cm^{-1}) is the linear and μ_m (cm^2/g) is the mass attenuation coefficients, respectively.

MAC can be also determined by Eq. 4 (Jackson and Hawkes, 1981);

$$\mu/\rho = \sum_i w_i (\mu/\rho)_i \tag{4}$$

w_i is the weight fraction and $(\mu/\rho)_i$ is the MAC of the i_{th} constituent element.

ACS (σ_a) can be obtained by the equation formulated as;

$$ACS = \sigma_a = \frac{N}{N_A}(\mu/\rho) \tag{5}$$

N_A is the Avogadro's number and N is the atomic mass of materials.

ECS (σ_e) is found by the equation (Han & Demir 2009a);

$$ECS = \sigma_e = \frac{\sigma_a}{Z_{eff}} \tag{6}$$

Z_{eff} can be found by Eq. 7 (Manohara and Hanagodimath, 2007).

$$Z_{eff} = \sigma_a/\sigma_e \tag{7}$$

HVL and MFP are calculated by Eqs. 8-9;

$$HVL = \frac{ln(2)}{\mu} \tag{8}$$

$$MFP = \frac{1}{\mu} \tag{9}$$

EBF and EABF can be obtained by the equations below (Harima et al. 1986; Harima, 1993). Geometric progression (G-P) fitting parameters for the alloy are determined by in Eq. 11 (ANSI/ANS, 1991). Buildup factors can be determined by Eq. 12 and 13, determining $K(E,x)$ in Eq. 14.

$$Z_{eq} = \frac{Z_1(logR_2 - logR) + Z_2(logR - logR_1)}{logR_2 - logR_1} \tag{10}$$

$$F = \frac{F_1(logZ_2 - logZ_{eq}) + F_2(logZ_{eq} - logZ_1)}{logZ_2 - logZ_1} \tag{11}$$

$$B(E,x) = 1 + \frac{(b-1)(K^x - 1)}{(K-1)} \quad \text{for} \quad K \neq 1 \tag{12}$$

$$B(E,x) = 1 + (b-1)x \quad \text{for } K = 1 \tag{13}$$

$$K(E,x) = cx^a + d\frac{tanh\left(\frac{x}{X_k} - 2\right) - tanh(-2)}{1 - tanh(-2)} \text{for } x \leq 40 \text{ mfp} \tag{14}$$

The R_1 and R_2 values are the $(\mu_m)_{Compton}/(\mu_m)_{Total}$ the adjacent elements with Z_1 and Z_2 atomic numbers. F is the (G-P) fitting parameters (a, b, c, d, X_K coefficients) of the sample. F_1 and F_2 are the G-P fitting parameters for Z_1 and Z_2 atomic numbers at an energy, respectively. X and E are penetration depth and primary photon energy, respectively.

The FNRCS ($\sum_R$) value of the material is determined as follows (Sakar, 2020; Woods, 2013):

$$\sum_R = \sum_i \rho_i (\sum_R/\rho)_i \tag{15}$$

where ρ_i is the partial density of the compound and $(\sum_R/\rho)_i$ is the mass RCS of the i_{th} constituent element.

3. Results

Based on the chemical components of EHEAs were taken from literature (Table 1) and the photon-matter interaction parameters of the alloys were determined. Dependences of the found MAC values versus photon energies (1keV-100GeV) are given in Fig. 1(a). At low (1-100keV), mid (100keV–5MeV) and high (>5 MeV) energies MAC values decreased apparently with increasing energy, a little changed and increased with increasing energy under the effect of the photoelectric (PE), Compton scattering (CS) and pair production (PP), respectively. XCom was also used to calculate the MAC values of the EHEAs to see the agreement of the results by Phy-X/PSD (Fig. 1). The MAC values of the RHE alloys and formerly studied super alloys for several energies are given in Table 2.

Table 1. Chemical compositions of the studied EHEAs.

Sample/Sample code	CoCrFeNiNb0.25Ta0.20 /D1	CoCrFeNiTa0.4 /D2	CoCrFeNiTa0.75/D3	CoCrFeNiTa0.25Hf0.25/D4	Co2MoxNi2VWx/D5
Co	22.28	22.81	21.1	21.80	25.74
Fe	22.53	21.45	21.1	22.03	-
Nb	4.900	-	-	-	-
Ta	4.500	12.64	15.6	5.480	-
Ni	22.56	21.44	21.1	22.07	19.62
Cr	23.23	21.66	21.1	22.77	-
Hf	-	-	-	5.860	-
W	-	-	-	-	23.60
V	-	-	-	-	10.19
Mo	-	-	-	-	20.85
Density	8.709	9.572	9.897	9.258	13.155

Variation of the calculated LAC values as a function of photon energies (1keV-100GeV) is given in Fig. 1(c). LAC is the parameter used for obtaining MAC, HVL and MFP parameters. Due to the density effect, bigger differences are observed for LAC values. D5 alloy has the biggest LAC value while D1 alloy has the lowest one at the same energy.

The HVL and MFP are the other parameters related to thickness. HVL and MFP values varying as a function of energies calculated by the code are seen in Fig. 2. At the energies dominant by CS, most photons have a high probability of scattering. So, thicker materials are required because their absorption probability is lower and the MFP of photons is longer. Having lower values of HVL and MFP at high energies indicates better shielding capability. The HVL values in the same energy region are ordered as D5<D3<D2<D4<D1. The ascending order of MFP

values is D5<D3<D2<D4<D1. Based on the found results, alloy D5 has the lowest HVL and MFP values, whereas D1 alloy has the highest ones. Therefore, it can be noted that D5 has the highest shielding feature among the alloys. The shielding capacity of the EHEAs are analyzed by the comparison of HVL values with those of previously given alloys and shown in Fig. 2(b).

The probability of interaction per electron and per atom per unit volume of a material is named as ECS and ACS, respectively. Varying of ECS and ACS results as a function of photon energies are seen in Fig. 3. If the alloy has greater values of ACS and ECS, it can be considered as a better protective alloy. Based on the values of ACS and ECS, the shielding potential of the D5 alloy is the highest among them.
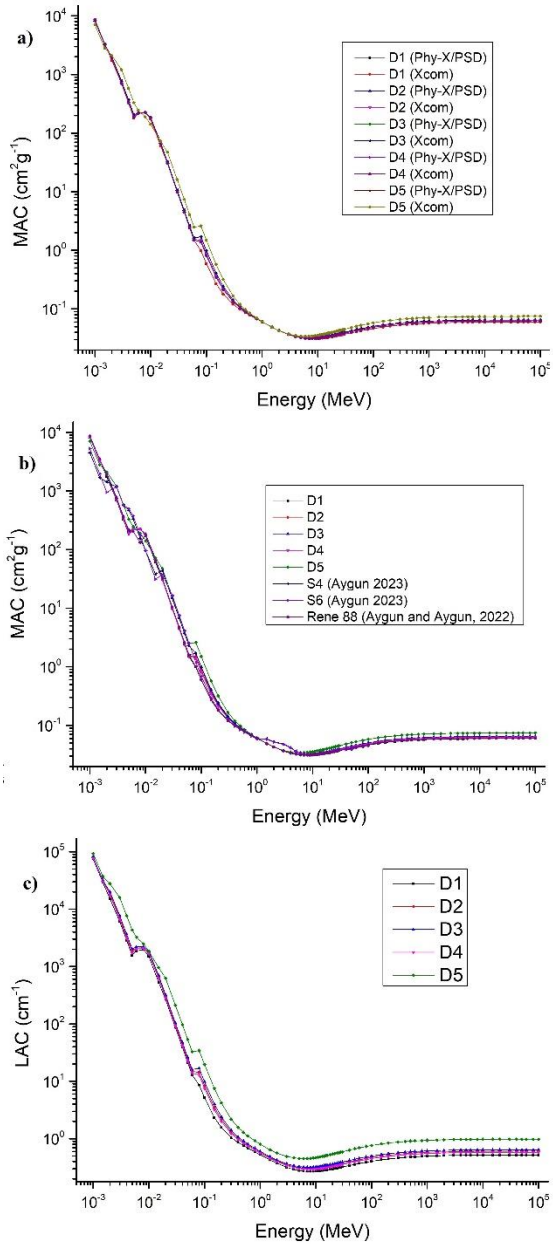
Figure 1. The variations of MAC (a) MAC of other alloys (b) and LAC (c) values versus photon energies.

Z_{eff} values varying versus photon energies are seen in Fig. 4. PE effect causes maximum Z_{eff} values at low energies. The highest Z_{eff} at ≈0.005 MeV can be observed by the K-absorption edge of Cr and that at ≈0.07 MeV can be observed for K-absorption edge of Ta and W as seen in Fig. 4. The values decreased apparently, then increased with increasing energy and stayed constant in the higher energies. The highest Z_{eff} values are achieved for D5 with the presence of W and Mo (higher atomic numbers); whereas lowest

Z_{eff} values are observed for D1 with no contribution of Hf, Mo and W. Thus, D5 alloy shows the highest shielding potential, while D1 shows the lowest shielding property.
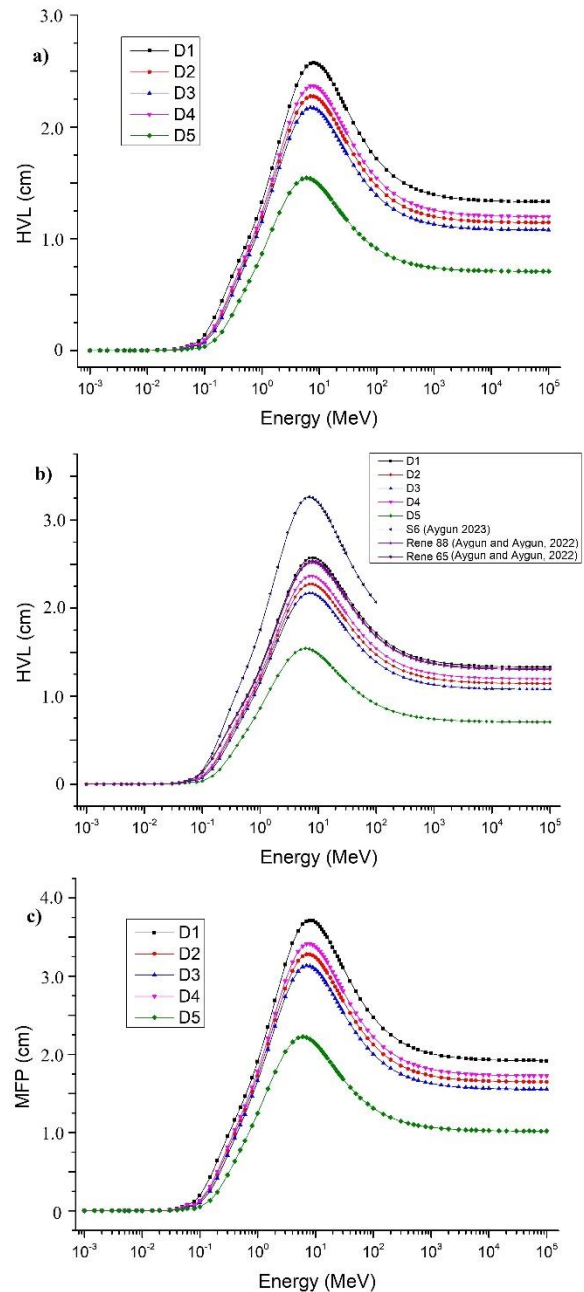
Figure 2. The variations of HVL (a) HVL of other alloys (b) and MFP (c) values versus photon energies.
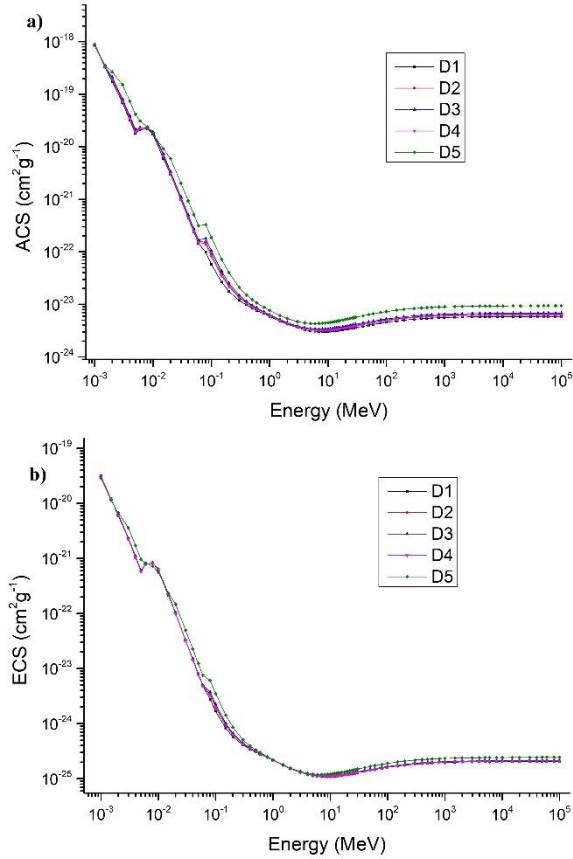
Figure 3. The variations of ACS (a) and ECS (b) values versus incident energy.
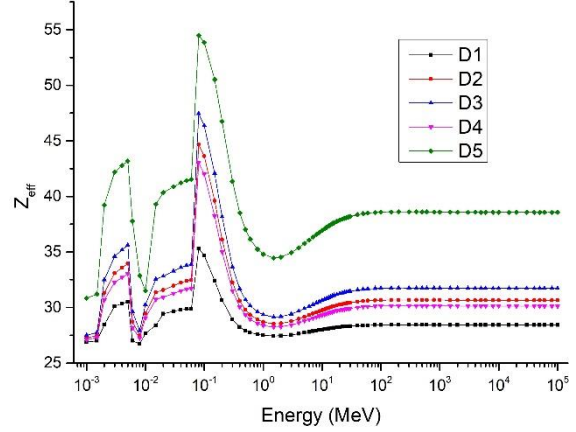
Figure 4. The variations of Z_{eff} values versus incident energy.

Table 2. Comparison of the MAC values for the EHEAs and previously reported alloys.

Energy (MeV)	D1	D2	D3	D4	D5	Rene 80 (Aygun and Aygun, 2022)	Rene 95 (Aygun and Aygun, 2022)	Inc 617 (Aygun and Aygun, 2023)	Inc 800HT (Aygun and Aygun, 2023)	In625 (Sayyed et al. 2020)	In718 (Sayyed et al. 2020)
0.015	60.61	68.41	70.62	67.03	72.63	64.38	63.06	59.14	60.60	65.70	59.00
0.03	9.957	10.17	10.56	9.931	16.12	10.44	10.83	10.83	8.763	9.549	10.41
0.05	2.420	2.498	2.607	2.432	4.047	2.537	2.633	2.626	2.101	2.287	2.51
0.8	0.068	0.069	0.069	0.068	0.070	0.068	0.068	0.068	0.067	0.068	0.067
1	0.060	0.061	0.061	0.061	0.061	0.061	0.061	0.060	0.060	0.061	0.060
3	0.036	0.037	0.037	0.037	0.037	0.037	0.037	0.037	0.036	0.037	0.037
5	0.032	0.033	0.033	0.033	0.034	0.033	0.033	0.032	0.032	0.032	0.032
8	0.031	0.032	0.032	0.032	0.036	0.031	0.032	0.031	0.030	0.031	0.031
10	0.031	0.032	0.033	0.032	0.036	0.032	0.032	0.031	0.030	0.031	0.031
100	0.046	0.049	0.050	0.049	0.058	0.047	0.047	0.046	0.044	-	-
1000	0.057	0.060	0.062	0.060	0.071	0.058	0.058	0.057	0.054	-	-
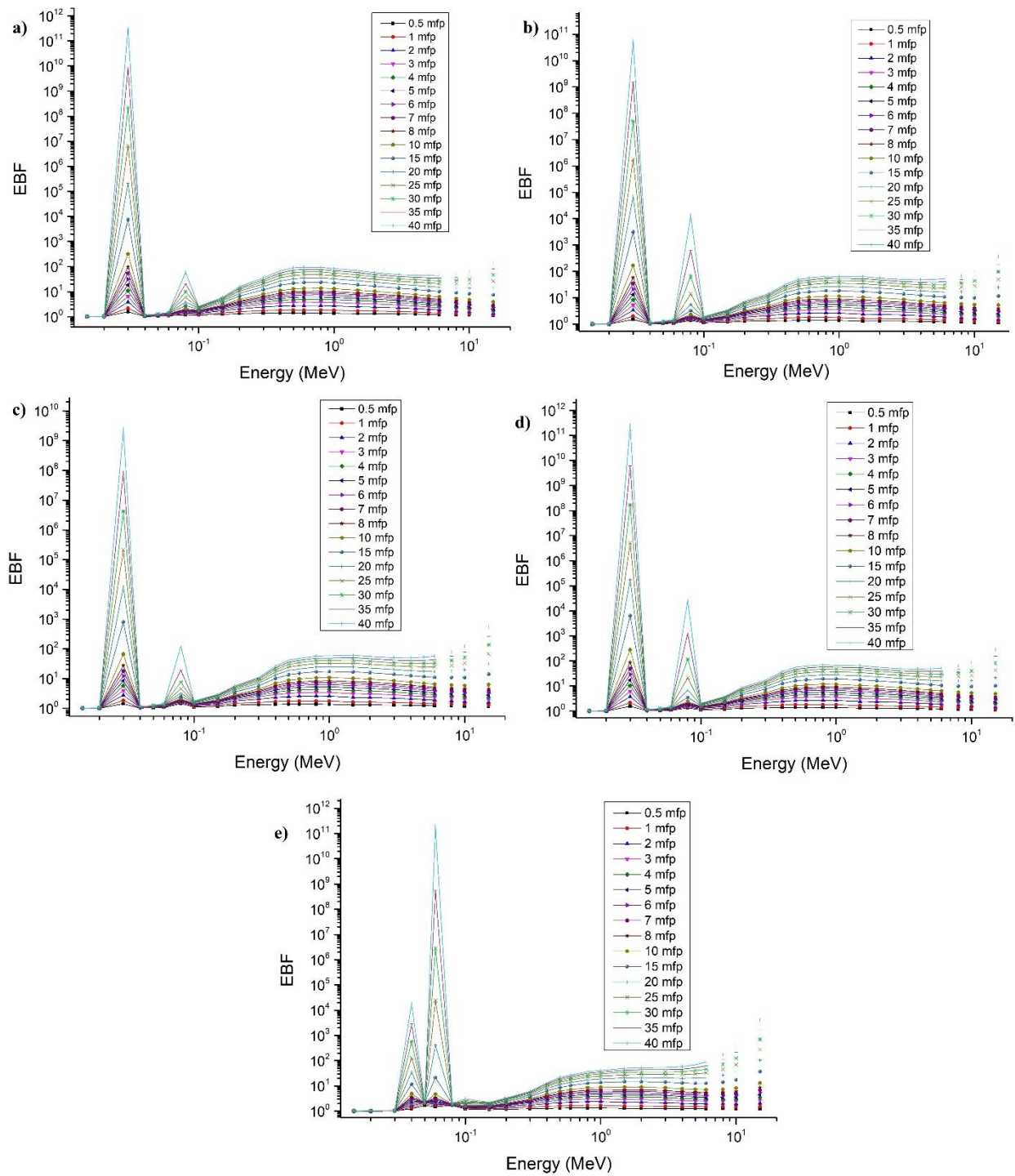
Figure 5. The variations of EBF values of D1 (a) D2 (b) D3 (c) D4 (d) D5 (e) versus photon energies.
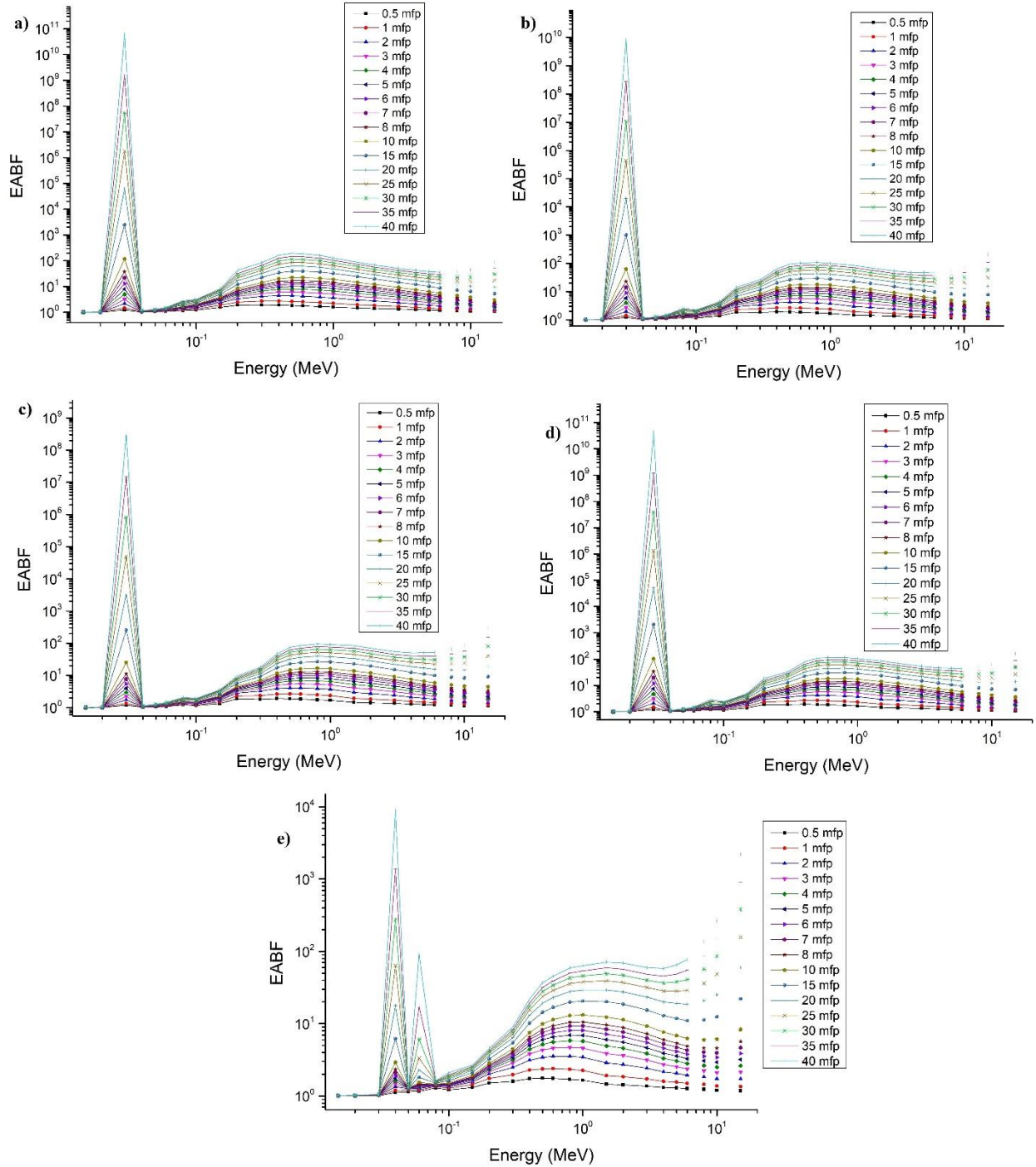
Figure 6. The variations of EABF values of D1 (a) D2 (b) D3 (c) D4 (d) D5 (e) versus photon energies.

EABF and EBF of the EHEAs were obtained for 16 penetration depths by Phy-X/PSD. The changes of buildup factors versus photon energies are given in Figs. 5-6. In PE region, buildup factors are small due to the fact that photons with low-energies are absorbed by their all energies. In CS region, since the large number of photons are scattered, photon accumulation increased and the factors achieve highest values in the mid-energy region. In PP region, photons are absorbed strongly. Hereby, the buildup factors have lower values at high energies. Depending on the values of EABF and EBF, the lowest photon cluster is observed for D5 EHEA than the other

alloys. The peak observed at ≈0.07 MeV can be due to K-absorption edge of Ta or W (Aygun, 2023).

FNRCS values of the EHEAs were determined and given in Fig. 7. It can be said that the highest value is obtained for D5 and the lowest one is for D1.
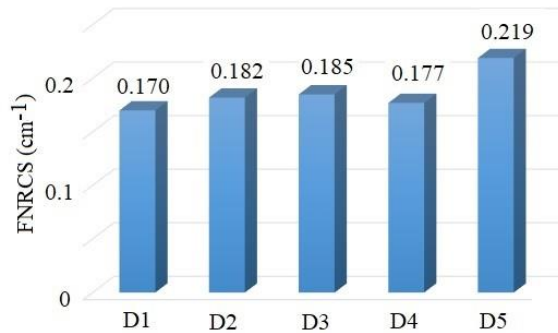
Figure 7. FNRCS values of the EHEAs.

4. Conclusions

In the paper, photon protection parameters of EHEAs were calculated by Phy-X/PSD code in the energies of 1 keV-100 GeV to learn the photon protection abilities. Xcom was also used for obtaining MAC values and it is seen that the results are compatible. It was examined that HVL values of the EHEAs are lower than those of previously reported alloys. It can be also mentioned that $Co_2Mo_xNi_2VW_x$ has highest shielding ability than the others, while $CoCrFeNiNb_{0.25}Ta_{0.20}$ has the lowest shielding property among the alloys. In general, the shielding performances of the alloys can be ordered as D5>D3>D2>D4>D1. Obtained FNRCS values make possible to use the alloys also for neutron shielding. Consequently, it is north worthy to say that the EHEAs can be estimated as new kind of shielding materials in radiation related areas with their superior features.

References

AYGUN, Z. (2023) Study on Radiation Shielding Characteristics of Refractory High Entropy Alloys by EpiXS Code. *Acta Physica Polonica A* 1(143):66-74.

AYGUN, Z., AYGUN, M., (2023). Evaluation of radiation shielding potentials of Ni-based alloys, Inconel-617 and Incoloy-800HT, candidates for high temperature applications especially for nuclear reactors, by EpiXS and Phy-X/PSD codes, *J. Polytech.* in press (2023). https://doi.org/10.2339/politeknik.1004657

AYGUN, Z., AYGUN, M., (2022). Radiation Shielding Potentials of Rene Alloys by Phy-X/PSD Code. *Acta Phys. Polonica A* 5(141), 507-515.

BERGER, M.J., HUBBELL, J.H., 1987. XCOM: Photon Cross Sections Database, Web Version 1.2. National Institute of Standards and Technology Gaithersburg, MD 20899, USA (available at. http://physics.nist.gov/xcom).Jackson, D.F., Hawkes, D.J., 1981. X-ray attenuation coefficients of elements and mixtures, *Physics Reports*, 70, 169–233.

CANTOR, B., CHANG, I.T.H., KNIGHT, P., VINCENT, A.J.B., (2004). Microstructural development in equiatomic multicomponent alloys. *Mater. Sci. Engineer. A*, 213, 375–377.

CHEN, Y., CHEN, D., WEAVER, J., GIGAX, J., WANG, Y., MARA, N.A., FENSIN, S., MALOY, S.A., MISRA, A., LI, N., (2023). Heavy ion irradiation effects on CrFeMnNi and AlCrFeMnNi high entropy alloys. *J. Nucl. Mater.*, 574, 154163.

HAN, I. & DEMIR, L. (2009). Studies on effective atomic numbers, electron densities from mass attenuation coefficients in TixCo1-x and CoxCu1-x alloys. *Nucl. Instr. Methods B*, 267, 3505–3510.

HAN, I. & DEMIR, L. (2010). Studies on effective atomic numbers, electron densities and mass attenuation coefficients in Au alloys. *J. X-ray Sci. Tech.*, 18, 39–46.

HARIMA, Y., SAKAMOTO, Y., TANAKA, S., KAWAI, M., (1986). Validity of geometric progression formula in approximating gamma-ray buildup factors. *Nucl. Sci. Engineer.* 94, 24–35.

HARIMA, Y., (1993). An historical review and current status of buildup factor calculations and applications. Radiat. Phys. Chem. 41, 631–672.ANSI/ANS 6.4.3. Gamma-ray Attenuation Coefficients and Buildup Factors for Engineering Materials. American

Nuclear Society, La Grange Park, Illinois, (1991).

JIANG, H., ZHANG, H., HUANG, T., LU, Y., WANG, T., LI, T., (2016). Microstructures and mechanical properties of Co2MoxNi2VWx eutectic high entropy alloys. *Mater. Design*, 109, 539–546.

JIANG, H., HAN, K., QIAO, D., LU, Y., CAO, Z., LI, T., (2018). Effects of Ta addition on the microstructures and mechanical properties of CoCrFeNi high entropy alloy. *Mater. Chem. Phys.*, 210, 43-48.

JIAO, W., MIAO, J., LU, Y., CHEN, X., REN, Z., YIN, G., LI, T., (2023). Designing CoCrFeNi-M (M = Nb, Ta, Zr, and Hf) eutectic high-entropy alloys via a modified simple mixture method. *J. Alloys Comp.*, 941, 168975.

JIE, Z.J., CAO, J.C., RUAN, Z.Q., LI, H.H., (2014). A promising new class of high-temperature alloys: eutectic high-entropy alloys. *Sci. Rep.,* 4, 6200.

LI, S,, CHEN, F., TANG, X., GE, G., SUN, Z., GENG, Z., FAN, M., & HUANG, P., (2022). Effect of Ti on the Microstructure and Mechanical Properties of AlCrFeNiTix Eutectic High-Entropy Alloys. *J Mater. Engineer. Perform*, 31, 8294–8303.

LU, Y.P., DONG, Y., GUO, S., JIANG, L., KANG, H.J., WANG, T.M., WEN, B., WANG, CHEN, X., XIE, W., ZHU, J., WANG, Z., WANG, Y., MA, Y., YANG, M., JIANG, W., YU, H., WU, Y., & HUI, Y., (2021). Influences of Ti Additions on the Microstructure and Tensile Properties of AlCoCrFeNi2.1 Eutectic High Entropy Alloy. *Intermetallics*, 128, 107024.

MANOHARA, S.R., HANAGODIMATH, S.M. (2007). Studies on effective atomic numbers and electron densities of essential amino acids in the energy range in energy range 1 keV-100 GeV. *Nucl Instrum. Methods B* 258, 321-328.

MUKARRAM, M., MUJAHİD, M., YAQOOB, K., (2021). Design and development of CoCrFeNiTa eutectic high entropy alloys. *J. Mater. Res.Tech.*, 10, 1243-1249.

SAKAR, E., (2020). Determination of photon-shielding features and build-up factors of nickel–silver alloys. *Radiat. Phys. Chem.* 172, 1-13.

SAKAR, E., OZPOLAT, O.F., ALIM, B., SAYYED, M.I., KURUDIREK, M., 2020. Phy-X / PSD: Development of a user friendly online software for calculation of parameters relevant to radiation shielding and dosimetry. *Radiat. Phys. Chem.* 166, 108496.

SAKAR, E. GULER, O., ALIM, B., SAY, Y., DIKICI, B., (2023). A comprehensive study on structural properties, photon and particle attenuation competence of CoNiFeCr-Ti/Al high entropy alloys (HEAs). *J. Alloys Comp.*, 931, 167561.

SAYYED, M., MOHAMMED, F.Q., MAHMOUD, K.; LACOMME, E., KAKY, K.M., KHANDAKER, M.U., FARUQUE, M.R.I. (2020). Evaluation of Radiation Shielding Features of Co and Ni-Based Superalloys Using MCNP-5 Code: Potential Use in Nuclear Safety. *Appl. Sci.* 10, 7680.

WANG, Y., LI, S., CHEN, F., YANG, K., GE, G., TANG, X., FAN, M., HUANG, P., (2023). Unique dislocation loops distribution of AlCrFeNiTix eutectic high-entropy alloys under high-temperature ion irradiation, *J. Alloys Comp.*, 170373.

WOOD, J. Computational methods in reactor shielding, Elsevier (2013).

XIANG, C., HAN, E.H., ZHANG, Z.M., FU, H.M., WANG, J.Q., ZHANG, H.F., et al., (2019). Design of single-phase high-entropy alloys composed of low thermal neutron absorption cross-section elements for nuclear power plant application. *Intermetallic* 104, 143-53.

XIAO, J.-K., TAN, H., CHEN, J., MARTINI, A., ZHANG C., (2020). Effect of carbon content on microstructure, hardness and wear resistance of CoCrFeMnNiCx high-entropy alloys. *J. Alloy. Compd.*, 847, 156533.

YEH, B.J.W., CHEN, S.K., LIN, S.J., GAN, J.Y., CHIN, T.S., SHUN, T.T., TSAU, C.H., CHANG, S.Y., (2004). Nanostructured high-entropy alloys with multiple principal elements: novel alloy design concepts and outcomes *Advan. Engineer. Mater*., 6(5), 299-303.

Classification of Baby Cries Using Machine Learning Algorithms

Adem EKİNCİ[*1], Enver KÜÇÜKKÜLAHLI[2]

[1] *Düzce University, Mathematics Master's Degree Program, Düzceı, Turkiye,*
adem3ekinci@gmail.com (ORCID: 0009-0003-4702-4835)

[2] *Düzce University, Faculty of Engineering, Department of Computer Engineering, Düzceı, Turkiye,*
enverkucukkulahli@duzce.edu.tr (ORCID: 0000-0002-0525-0477)

Abstract

People are constantly engaged in communication with each other, and they mostly do so through language. The most effective form of communication for a newborn baby until they acquire this skill is crying. Although baby cries are often perceived as bothersome by adult individuals, they can contain a wealth of information. In this study, the information contained in infant cry signals was interpreted using audio processing methods and classified using machine learning algorithms. Feature extraction was performed on the dataset using the Mel Frequency Cepstral Coefficients (MFCC) method, and performance metrics were measured after using k-NN, SVM, Random Forest, and MLP classification algorithms

In the donate-a-cry dataset used in the study, before the feature extraction, the data was divided into 10 equal parts to increase the number of data and it has been observed that this method increases the classification success. For instance the k-NN algorithm achieved a performance value of 85.78% before the method was applied then after the method was applied, the performance value increased by 13.11% and reach 98.88%.

Keywords: Baby cries, Machine learning, SVM, Random Forest, MLP, k-NN

1. Introduction

Crying is an innate response observed in all babies and serves as an effective means of communication for them. They can express their hunger, discomfort, sleeplessness, or when something is amiss through crying. Therefore, a baby's cry is one of the most important signals that caregivers need to pay attention to. When the indicated situation is understood correctly and the issues are addressed, babies become happier, which positively impacts their healthy development (Lahti et al., 2019). In this regard, it is crucial to identify the reason quickly and accurately behind a baby's crying. Mothers, experienced caregivers, or healthcare professionals may be competent in this regard, but not always. A father who doesn't spend much time with the baby, an inexperienced caregiver, or a healthcare professional may struggle to understand the cause of crying, which can prolong the duration of crying. Prolonged crying in babies leads to an increase in cortisol levels, which can have negative effects on the brain and cognitive functions (Halpern & Coelho, 2016). Therefore, flawless and prompt methods should be preferred to quickly stop crying by meeting the baby's genuine needs. In this respect the main purpose of this study is to determine the cause of baby crying with higher accuracy using machine learning. Considering that baby crying is a sound signal, sound processing can provide more effective results in this context.

Not every sound we hear in our daily lives carries meaning to us. An unknown language, the sound of a bird, or a baby crying. However, when these sounds are recorded and analyzed using sound processing methods, it is observed that they carry more information than what we perceive. Sound processing fundamentally involves operations such as organizing sound signals, reducing noise, conducting spectral

analysis, filtering, visualization, and feature extraction (Purwins et al., 2019). Feature extraction is the process of distinguishing the significant characteristics of data in a dataset. Features emerge from the differences in time, frequency, and other properties of sound data. Various methods can be employed for feature extraction, including Mel Frequency Cepstral Coefficients (MFCC), Linear Predictive Coding (LPC), and Short-Time Fourier Transform (STFT) (Ji et al., 2021; Rezaee et al., 2023a). After this process, the data containing sound becomes compatible with machine learning algorithms. Consequently, numerous operations such as speech recognition, speaker recognition, emotion detection, disease diagnosis, and music recognition can be performed.

Machine learning is one of the most significant branches of artificial intelligence. It involves creating and developing systems that acquire learning capabilities by analyzing data or experiences. Machine learning algorithms are trained on datasets, and the quality, diversity, size, and accuracy of the data directly impact the performance of the algorithms. Therefore, the dataset serves as the fundamental basis for machine learning (Zhou, 2021).

Insufficient data in a dataset can lead to overfitting or a decrease in the model's generalization ability. Data augmentation methods can be employed to prevent such situations. Data augmentation techniques involve manipulating existing data to generate new data (Zhou, 2021). Some well-known data augmentation methods include random cropping, random shifting, mirroring, rotation, time stretching, and others (Huang et al., 2019).

A baby's crying is essentially a sound signal. Like other sound signals, it has a specific frequency, tone, and intensity. Any operation used in sound processing can be applied to these sound signals. Feature extraction is one of these operations. Baby cry signals with extracted features can be processed using machine learning. Thus, a machine learning model trained with sufficient data and the right methods can accurately identify the reasons why babies cry. Although the notion of Gröbner basis firstly handled with the current name by Buchberger in his PhD thesis (Buchberger 1965), in 1927, Macaulay had been used this idea in his famous paper (Macaulay 1927).

2. Related Work

In a study conducted by Michelsson and colleagues, the analysis of newborn infants' crying sounds using spectrographic analysis was discussed, highlighting the differences between healthy and sick infants (Michelsson & Michelsson, 1999).

Sharma and colleagues achieved an accuracy of 81.27% using Gaussian mixture model clustering for the Donate-a-cry dataset (Sharma et al., 2019).

Kulkarni and colleagues classified infant cries using various features such as MFCC, Spectral Flatness, GTCC, STACF, Spectral Roll-off, etc., along with LR, SVM, k-NN, and RF algorithms, obtaining an accuracy of 84% with MFCC and LR combination (Kulkarni et al., 2021).

Dewi and colleagues compared the performance of MFCC and LFCC for infant cry samples using the K-NN algorithm, finding that LFCC was more effective (Dewi et al., 2019).

Sutanto and colleagues discussed an Internet of Things (IoT)-based baby incubator monitoring system to identify infant cries and monitor their health conditions, utilizing the donate-a-cry dataset (Sutanto et al., 2021).

Messaoud and colleagues achieved a 71.4% accuracy by segmenting 1615 sound samples from 13 infants and using the MFCC method with PNN (Messaoud & Tadj, 2010).

Izmirli employed a spectral flatness-based audio segmentation method in their study (Izmirli, 2000).

Bashiri and colleagues achieved a 99.9% accuracy using the MFCC and ANN algorithms with the Baby-Chilanto dataset (Bashiri & Hosseinkhani, 2020). Other studies using the same dataset include Hariharan et al., who achieved 99% accuracy with STFT-GRNN (Hariharan et al., 2012), Hariharan et al., who obtained 99.49% accuracy with Wavelet Packets-PNN (Hariharan et al., 2011), and Sahak et al., who achieved 95.07% accuracy with BPSO-ANN (Sahak et al., 2010).

In a study by Razaee and colleagues, using the donate-a-cry dataset and the deep-SVM algorithm with a segmentation method, an accuracy of 98.4% was obtained (Rezaee et al., 2023b).

Apart from the Baby-Chilanto and donate-a-cry datasets, some studies in the literature have utilized the Dunstan Baby Language dataset for baby sound classification (Bănică et al., 2016; Franti et al., 2018; Maghfira et al., 2020).

3. Material

3.1. Dataset

Donate-a-cry is created through parents recording their children's crying sounds and relevant information using a mobile application installed on IOS and Android smartphones. The contributors who uploaded the audio recording also labeled the crying according to the given instructions and indicated the cause of crying they suspected. It was initially published on the GitHub platform by Gaber Veres in 2015 (Veres, 2015/2023). The dataset was later updated, applying preliminary audio processing steps to each recording. The sound files consist of baby cries ranging from 1 to 22 months. The files have a frequency of 1800 and a bitrate value of 128 kbps. The updated version of the dataset was used in this study. The distribution of data into classes is provided in Table 1. The database is published under the ODbL.

Reason	Records
Belly pain	16
Burping	8
Discomfort	27
Hungry	382
Tired	24
Total	457

Table 1 The distribution of classes in the Donate-a-cry dataset.

3.2. Feature Extraction

Feature extraction is essentially creating numerical representations that capture the important characteristics of the sound. In this study, Mel-Frequency Cepstral Coefficients (MFCC) were used for feature extraction.

MFCC (Mel-Frequency Cepstral Coefficients) is a representation of the short-term power spectrum of a sound signal on the Mel scale, which represents the perceptual changes in human hearing of sound frequencies (Figure 2). The MFCC method divides the sound signal into short time frames and performs a power spectrum analysis (Figure 1) for each frame. In this analysis, the energy of the sound in different frequency bands is calculated and weighted in a manner similar to the frequency sensitivity of the human ear. Subsequently, logarithmic processing and Discrete Cosine Transform (DCT) are applied to transform the frequency scale, resulting in the extraction of MFCC coefficients. These coefficients represent different features of the sound signal and can be used in various applications such as speech recognition, speaker identification, and music classification.
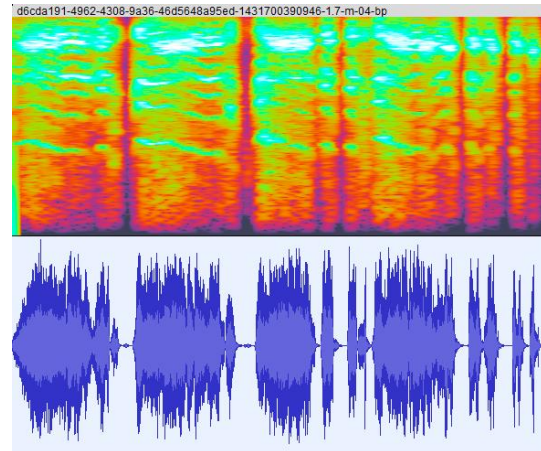
Figure 1 A sound signal and its spectrogram from the Belly pain class.

MFCC consists of the following steps (Tiwari, n.d.):

- First, the sound signal is converted from analog to digital, and the sampling frequency is determined.

- Then, the sound signal is passed through a pre-emphasis filter. This filter enhances the energy in high frequencies and improves speech recognition performance.

$$y[n] = x[n] - \alpha\, x[n-1]$$

where $y[n]$ is the filtered signal, $x[n]$ is the input signal, and α is the pre-emphasis coefficient.

- Next, the sound signal is divided into short time intervals called frames. Typically, a frame length of 25 ms and a frame shift of 10 ms are used. A Hamming or Hanning window is applied to the frames to prevent abrupt transitions between frames.

$$w[n] = 0.54 - 0.46 \cos\left(\frac{2\pi n}{N-1}\right)$$

where, $w[n]$ is the window function, n is the frame index, and N is the frame length.

- Then, the spectrum is calculated for each frame. The spectrum represents the frequency components of the sound signal. Fast Fourier Transform (FFT) is used to calculate the spectrum.

$$X[k] = \sum_{n=0}^{N-1} x[n] e^{\frac{-j2\pi kn}{N}}$$

where, $X[k]$ is the spectrum, $x[n]$ is the time signal, N is the frame length, and k is the frequency index.

- The spectrum is then weighted by a Mel-filter bank. The Mel-filter bank consists of a series of triangular filters that mimic the frequency scale perceived by the human ear.

$$H_m(k) = \begin{cases} 0 & k < f(m-1) \\ \frac{k-f(m-1)}{f(m)-f(m-1)} & f(m-1) \le k < f(m) \\ \frac{f(m+1)-k}{f(m+1)-f(m)} & f(m) \le k < f(m+1) \\ 0 & k \ge f(m+1) \end{cases}$$

where, $H_m(k)$ is the value of the $m-th$ filter at the $k-th$ frequency, and $f(m)$ is the center frequency of the $m-th$ filter.

- Finally, the logarithm of the spectrum passed through each filter is taken, and the inverse Fourier transform is applied to obtain the MFCC.

$$E = \sum_{n=0}^{N-1} x^2[n]$$

where, E is the energy and $x[n]$ is the time signal.
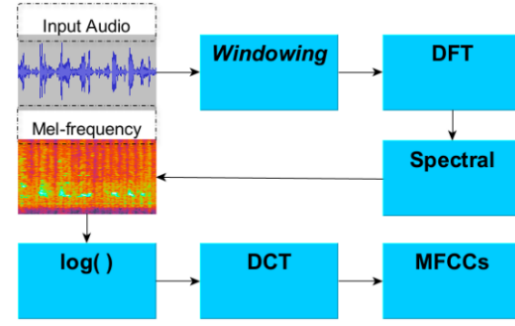
Figure 2 MFCC process diagram.

3.3. Machine Learning

Machine learning, one of the most used subfields of artificial intelligence, has found its place in many studies related to the classification of baby cries. In this study, four different classification algorithms of machine learning were modeled, and their classification performances were examined.

3.3.1. Random Forest

Random forest algorithm is a powerful and flexible machine learning technique used in supervised learning. This algorithm can solve classification or regression problems by combining multiple decision trees. It is based on the concept of ensemble learning, which involves aggregating multiple classifiers together to improve model performance and solve complex problems.

During training, the algorithm constructs multiple decision trees and works by determining the class that is most frequent (for classification) or the average prediction (for regression) among the individual tree's classes. The decision trees are constructed using a random subset of features and data with replacement (bootstrapping). This introduces randomness and diversity among the trees, reducing the correlation and variance of predictions (Probst et al., 2019).

3.3.2. Support Vector Machine (SVM)

SVM is a supervised learning algorithm used for classification problems. The SVM algorithm draws a hyperplane to separate two or more classes. This hyperplane maximizes the margin, which is the gap between the two classes. The margin represents the distance between the closest points of the two classes.

The SVM algorithm can project data points into higher dimensions to expand the margin. It achieves this by using functions called kernels. Kernel functions measure how similar or distant data points are from each other. Different kernel models, such as Linear kernel, Polynomial kernel (Poly), Radial Basis Function (RBF) kernel, Sigmoid kernel, are available.

The SVM algorithm can be mathematically expressed as follows:

$$\min_{w,b} \frac{1}{2} \| w \|^2 + C \sum_{i=1}^{n} \xi_i$$

where w and b are the parameters of the hyperplane. The parameter C adjusts the balance between expanding the margin and reducing classification errors. ξ_i is a loss function that determines how much a data point enters the margin region or deviates from the correct class. This formula aims to optimize both the margin and the classification errors of the hyperplane (Pisner & Schnyer, 2020).

3.3.3. Multilayer Perceptron (MLP)

MLP (Multilayer Perceptron) is an important model in the context of the approximation theory within neural networks. It consists of an input layer, one or more hidden layers, and an output layer. Units (neurons) in each layer are interconnected with connections from the input layer to the output layer. The basic structure of an MLP is to process input data through the hidden layers using weights and activation functions to produce an output. In each hidden layer, the inputs are multiplied by weights, subjected to an activation function, and passed on to subsequent layers. This process is repeated as it passes through the hidden layers, ultimately resulting in an output in the output layer. The MLP model is used to capture complex and non-linear relationships in input data. This is done by employing various activation functions such as sigmoid, ReLU, tanh. The MLP adjusts its weights through a learning process that fits the data, and it can then make predictions on new data. The MLP has a wide range of applications and can achieve successful results in various problems such as pattern recognition, classification, regression, and time series analysis. Additionally, the presence of multiple hidden layers in an MLP allows for the learning of more complex relationships and features (Taud & Mas, 2018).

3.3.4. k-Nearest Neighbors (k-NN)

The k-NN (k-Nearest Neighbors) algorithm is a supervised learning method that predicts the class or value of a given instance based on its closest neighbors. The steps of this algorithm are as follows:

First, the k parameter is selected. This parameter represents the number of nearest neighbors to consider for a given instance. For example, if k=3, the closest 3 neighbors will be considered.
The distance between the given instance and other instances is calculated. Various distance measures can be used for this purpose, such as Euclidean distance, Manhattan distance, Minkowski distance, and so on.
Next, the distances are sorted in ascending order, and the k instances with the smallest distances are identified. These instances are referred to as the nearest k neighbors.
If the problem is a classification problem, the classes of the nearest k neighbors are examined, and the most commonly occurring class is predicted.
If the problem is a regression problem, the average of the target variable values of the nearest k neighbors is taken, and this value is presented as the prediction.
The k-NN algorithm is a simple and easy-to-implement method. However, it also has some disadvantages. For example, choosing the right value for the k parameter is important, as having a value that is too large or too small can reduce the accuracy. Additionally, computing distances with the entire dataset for each new instance can be computationally expensive in terms of time and memory (Kramer, 2013).

3.4. Performance Evaluation Scores

Confusion Matrix: It is a matrix used to evaluate the performance of a classification model and shows the number of correct and incorrect predictions made by the model. The confusion matrix consists of four main categories: True Positive (TP), False Positive (FP), True Negative (TN), and False Negative (FN). These categories indicate in which cases the classification model made correct or incorrect predictions.

Accuracy: Represents the ratio of correctly classified examples to the total number of examples. In other words, it shows the percentage of correctly classified examples among all the examples.

$$Accuracy = \frac{TP + TN}{TP + TN + FP + FN}$$

Precision: It is a value that indicates how many of the examples predicted as positive by a classification model are truly positive. In simpler terms, precision represents the ratio of correct positive predictions to the total positive predictions made by the model.

$$Precision = \frac{TP}{TP + FP}$$

Recall (Sensitivity): It is a metric that shows how much of the true positive examples a classification model correctly identifies. Recall is also referred to as "sensitivity".

$$Recall = \frac{TP}{TP + FN}$$

F1 Score: It is the harmonic mean of precision and recall metrics and helps evaluate the performance of the model from a broader perspective.

$$F1 = \frac{2 \times Precision \times Recall}{Precision + Recall}$$

4. Method

As a data augmentation method, each data in the dataset has been divided into 10 parts to create a second dataset. This method has been used for music genre classification in (Velardo, 2020). For each part in this resulting dataset, feature extraction is applied using MFCC (Mel-frequency cepstral coefficients). To apply MFCC, the audio signals of each part are divided into windows with a sampling rate of 22050 Hz and a 50% overlap. Windowing helps us visualize the time and frequency components of the signal better and reduces side effects in Fourier transformation. Then, a Mel-frequency filter bank and discrete cosine transformation are applied to each window. As a result, 13 MFCC coefficients are calculated for each part.
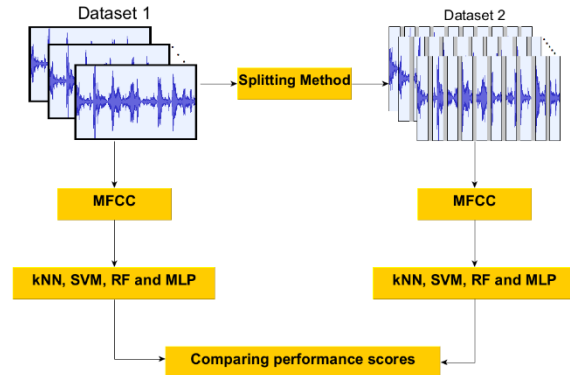
Figure 3 Flowchart of the model proposed

Using these generated MFCC coefficients, performance evaluation scores are calculated for the four metrics of the confusion matrix in algorithms.

Some important parameters used in the algorithms are provided in the table below:

	P1	P2	P3	P4
k-NN	k = 5	Distance = Minkowski	-	-
SVM	Kernel = RBF	c = 12	-	-
RF	Trees = 100	Tree Depth = 32	Criterion = Entropy	-
MLP	Alpha = 0.01	Max Iterations = 600	Hidden Layer Size = 12	Algorithm = LBFGS

To ensure more reliable and unbiased detection of each metric, a 10-fold cross-validation method is used. This method creates different training and test sets, utilizing the entire dataset and preventing data wastage. Also Each algorithm was run 30 times with the same parameters for result verification.

5. Findings

The scores identified in the study are provided in the tables 2 and 3 below. Table 2 has been examined for four algorithms. As seen in Table 2, using the data augmentation method, a 98.88% accuracy was achieved with the k-NN algorithm. The impact of the data augmentation method on the results is more clearly seen in Table 3. The performance values have

increased by 15.69% for SVM, 13.11% for k-NN, 11.91% for Random Forest, and 11.42% for MLP. Additionally, the confusion matrices for dataset1 and dataset2 are provided in Figures 4, 5, 6 and 7 for four algorithms.

		Accuracy Score	Recall (Sensitivity) Score	Precision Score	F1 Score
k-NN	Max	98,88%	98,88%	98,89%	98,89%
	Min	98,88%	98,88%	98,89%	98,89%
	Mean	**98,88%**	**98,88%**	**98,89%**	**98,89%**
SVM	Max	98,60%	98,60%	98,60%	98,60%
	Min	98,60%	98,60%	98,60%	98,60%
	Mean	**98,60%**	**98,60%**	**98,60%**	**98,60%**
Random Forest	Max	98,58%	98,88%	98,56%	98,54%
	Min	98,18%	98,18%	98,14%	98,13%
	Mean	**98,33%**	**98,33%**	**98,30%**	**98,29%**
MLP	Max	98,42%	98,42%	98,45%	98,44%
	Min	97,86%	97,86%	97,88%	97,86%
	Mean	**98,23%**	**98,23%**	**98,24%**	**98,23%**

Table 2 Performance scores obtained after running the algorithms 30 times.

	Accuracy Score for 10 Segments	One Piece Accuracy Score	Difference
k-NN	98,88%	85,78%	**13,11%**
SVM	98,18%	82,49%	**15,69%**
Random Forest	98,38%	86,47%	**11,91%**
MLP	98,60%	87,18%	**11,42%**

Table 3 The Impact of Data Augmentation Method on Performance Metrics
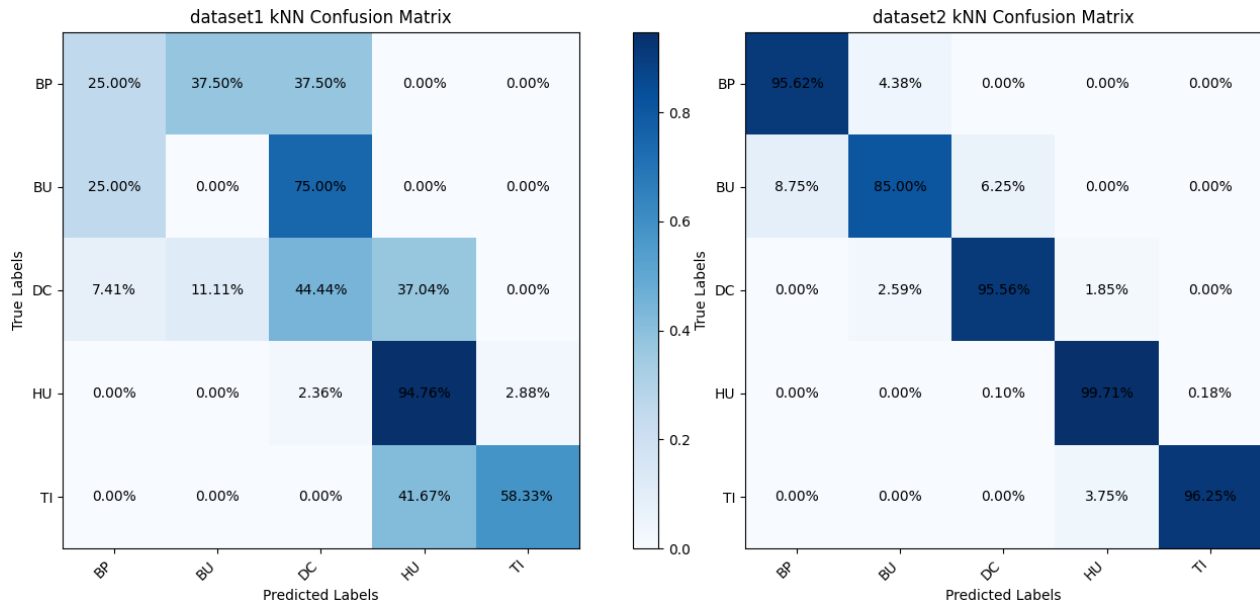
Figure 4: Confusion matrix of dataset1 and dataset2 with k-NN algorithm
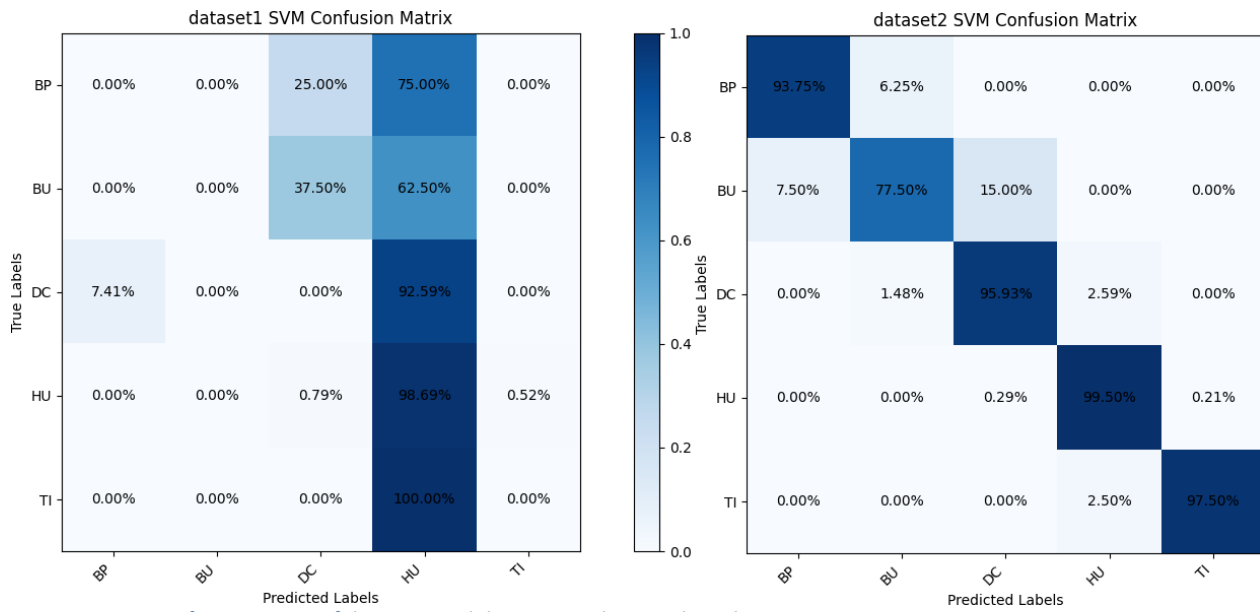
Figure 5:SVM Confusion matrix of dataset1 and dataset2 with SVM algorithm
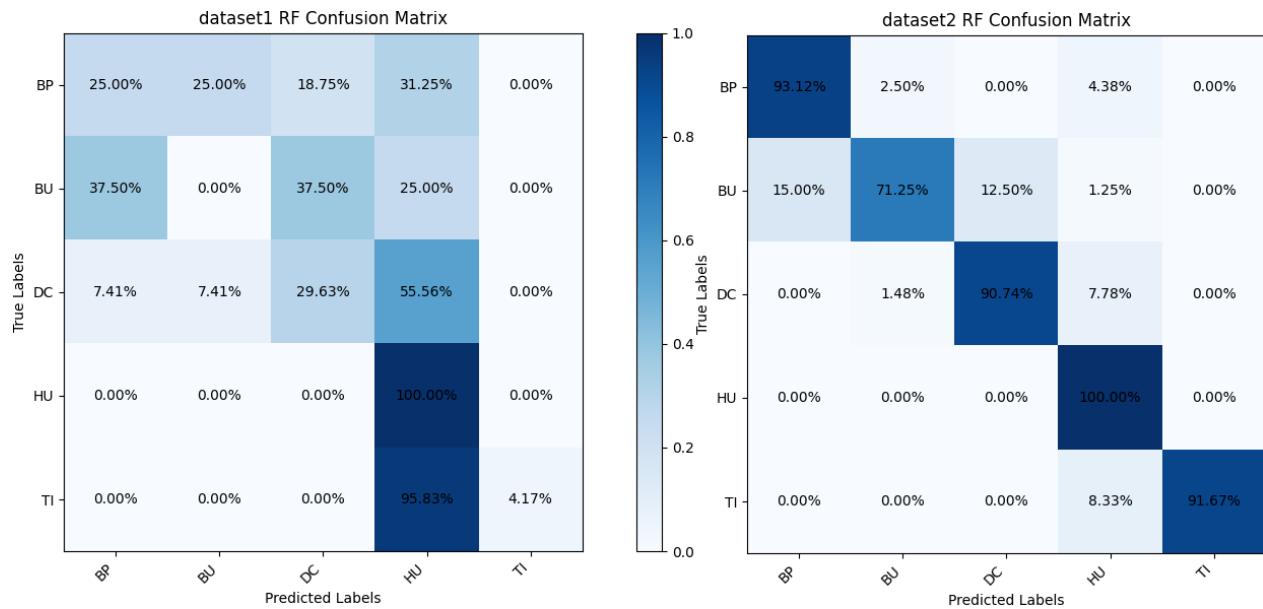
Figure 6: Confusion matrix of dataset1 and dataset2 with RF algorithm
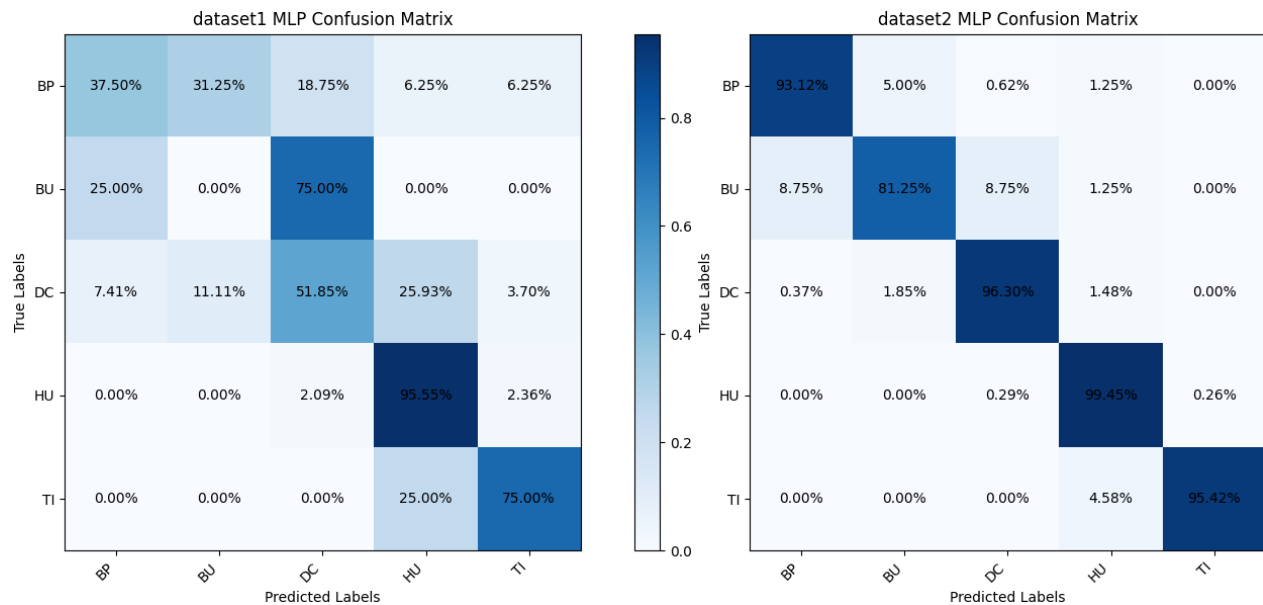
Figure 7: Confusion matrix of dataset1 and dataset2 with MLP algorithm

5. Discussion and Conclusions

In our study, the method of augmenting the size of the database through dividing the data into equal segments was employed for classification of baby cries which used in (Velardo, 2020) for music genre classification. The results indicate that this method has had a positive impact on identifying the causes of baby cries.

The Donate-a-cry dataset used in our study has also been employed in previous research (Sharma et al., 2019; Kulkarni et al., 2020; Sutanto et al., 2021; Rezaee et al., 2023b). Among these studies, the work by Rezaee et al. (2023b) achieved the highest performance with a deepSVM algorithm, reaching an accuracy of 98.34%. In this study, by employing data augmentation techniques and the k-NN algorithm, a performance of 98.88% was attained, surpassing the previous works that utilized the donate-a-cry dataset, thereby achieving the highest success rate.

Based on the performance scores, it has been considered as a strong assumption that the sound of baby's crying for a specific reason exhibits characteristic features even in small segments.

References

BĂNICĂ, I.-A., CUCU, H., BUZO, A., BURILEANU, D., & BURILEANU, C. (2016). Automatic methods for infant cry classification. 2016 International Conference on Communications (COMM), 51-54. https://doi.org/10.1109/ICComm.2016.752826 1

BASHIRI, A., & HOSSEINKHANI, R. (2020). Infant Crying Classification by Using Genetic Algorithm and Artificial Neural Network. Acta Medica Iranica, 531-539. https://doi.org/10.18502/acta.v58i10.4916

DEWI, S. P., PRASASTI, A. L., & IRAWAN, B. (2019). The Study of Baby Crying Analysis Using MFCC and LFCC in Different Classification Methods. 2019 IEEE International Conference on Signals and Systems (ICSigSys), 18-23. https://doi.org/10.1109/ICSIGSYS.2019.88110 70

FRANTI, E., ISPAS, I., & DASCALU, M. (2018). Testing the Universal Baby Language Hypothesis—Automatic Infant Speech Recognition with CNNs. 2018 41st International Conference on Telecommunications and Signal Processing (TSP), 1-4. https://doi.org/10.1109/TSP.2018.8441412

HALPERN, R., & COELHO, R. (2016). Excessive crying in infants. Jornal De Pediatria, 92(3 Suppl 1), S40-45. https://doi.org/10.1016/j.jped.2016.01.004

HARIHARAN, M., SINDHU, R., & YAACOB, S. (2012). Normal and hypoacoustic infant cry signal classification using time-frequency analysis and general regression neural network. Computer Methods and Programs in Biomedicine, 108(2), 559-569. https://doi.org/10.1016/j.cmpb.2011.07.010

HARIHARAN, M., YAACOB, S., & AWANG, S. A. (2011). Pathological infant cry analysis using wavelet packet transform and probabilistic neural network. Expert Systems with Applications, 38(12), 15377-15382. https://doi.org/10.1016/j.eswa.2011.06.025

HUANG, L., PAN, W., ZHANG, Y., QIAN, L., GAO, N., & WU, Y. (2019). Data Augmentation for Deep Learning-based Radio Modulation Classification (arXiv:1912.03026; Versiyon 1). arXiv. http://arxiv.org/abs/1912.03026

IZMIRLI, Ö. (2000, Ocak 1). Using a Spectral Flatness Based Feature for Audio Segmentation and Retrieval.

JI, C., MUDIYANSELAGE, T. B., GAO, Y., & PAN, Y. (2021). A review of infant cry analysis and classification. EURASIP Journal on Audio, Speech, and Music Processing, 2021(1), 8. https://doi.org/10.1186/s13636-021-00197-5

KRAMER, O. (2013). K-Nearest Neighbors. Içinde O. Kramer (Ed.), Dimensionality Reduction with Unsupervised Nearest Neighbors (ss. 13-23). Springer. https://doi.org/10.1007/978-3-642-38652-7_2

KULKARNI, P., UMARANI, S., DIWAN, V., KORDE, V., & REGE, P. P. (2021). Child Cry Classification—An Analysis of Features and Models. 2021 6th International Conference for Convergence in Technology (I2CT), 1-7. https://doi.org/10.1109/I2CT51068.2021.9418 129

LAHTI, K., VÄNSKÄ, M., QOUTA, S. R., DIAB, S. Y., PERKO, K., & PUNAMÄKI, R. (2019). Maternal experience of their infants' crying in the context of war trauma: Determinants and consequences. Infant Mental Health Journal, imhj.21768. https://doi.org/10.1002/imhj.21768

MAGHFIRA, T. N., BASARUDDIN, T., & KRISNADHI, A. (2020). Infant cry classification using CNN – RNN. Journal of Physics: Conference Series, 1528(1), 012019. https://doi.org/10.1088/1742-6596/1528/1/012019

MESSAOUD, A., & TADJ, C. (2010). A Cry-Based Babies Identification System. 6134, 192-199. https://doi.org/10.1007/978-3-642-13681-8_23

MICHELSSON, K., & MICHELSSON, O. (1999). Phonation in the newborn, infant cry. International Journal of Pediatric Otorhinolaryngology, 49 Suppl 1, S297-301. https://doi.org/10.1016/s0165-5876(99)00180-9

PISNER, D. A., & SCHNYER, D. M. (2020). Chapter 6—Support vector machine. Içinde A. Mechelli & S. Vieira (Ed.), Machine Learning (ss. 101-121). Academic Press. https://doi.org/10.1016/B978-0-12-815739-8.00006-7

PROBST, P., WRIGHT, M. N., & BOULESTEIX, A.-L. (2019). Hyperparameters and tuning strategies for random forest. WIREs Data Mining and Knowledge Discovery, 9(3), e1301. https://doi.org/10.1002/widm.1301

PURWINS, H., LI, B., VIRTANEN, T., SCHLÜTER, J., CHANG, S.-Y., & SAINATH, T. (2019). Deep Learning for Audio Signal Processing. IEEE Journal of Selected Topics in Signal Processing, 13(2), 206-219. https://doi.org/10.1109/JSTSP.2019.2908700

REZAEE, K., GHAYOUMI ZADEH, H., QI, L., RABIEE, H., & KHOSRAVI, M. R. (2023a). Can you Understand why I am Crying? A Decision-making System for Classifying Infants' Cry Languages Based on deepSVM Model. ACM Transactions on Asian and Low-Resource Language Information Processing. https://doi.org/10.1145/3579032

REZAEE, K., GHAYOUMI ZADEH, H., QI, L., RABIEE, H., & KHOSRAVI, M. R. (2023b). Can you Understand why I am Crying? A Decision-making System for Classifying Infants' Cry Languages Based on deepSVM Model. ACM Transactions on Asian and Low-Resource Language Information Processing. https://doi.org/10.1145/3579032

SAHAK, R., LEE, Y. K., MANSOR, W., YASSIN, A. I. M., & ZABIDI, A. (2010). Optimized Support Vector Machine for classifying infant cries with asphyxia using Orthogonal Least Square. 2010 International Conference on Computer Applications and Industrial Electronics, 692-696. https://doi.org/10.1109/ICCAIE.2010.5735023

SHARMA, K., GUPTA, C., & GUPTA, S. (2019). Infant Weeping Calls Decoder using Statistical Feature Extraction and Gaussian Mixture Models. 2019 10th International Conference on Computing, Communication and Networking Technologies (ICCCNT), 1-6. https://doi.org/10.1109/ICCCNT45670.2019.8944527

SUTANTO, E., FAHMI, F., SHALANNANDA, W., & ARIDARMA, A. (2021). Cry Recognition for Infant Incubator Monitoring System Based on Internet of Things using Machine Learning. International Journal of Intelligent Engineering and Systems, 14, 444-452. https://doi.org/10.22266/ijies2021.0228.41

TAUD, H., & MAS, J. F. (2018). Multilayer Perceptron (MLP). Içinde Geomatic Approaches for Modeling Land Change Scenarios (ss. 451-455). Springer, Cham. https://doi.org/10.1007/978-3-319-60801-3_27.

VERES, G. (2023). Donateacry-corpus. https://github.com/gveres/donateacry-corpus (Original work published 2015)

ZHOU, Z.-H. (2021). Machine Learning. Springer. https://doi.org/10.1007/978-981-15-1967-3

VELARDO, V. (2020). Deep Learning for Audio with Python, https://github.com/musikalkemist/DeepLearningForAudioWithPython/blob/master/12-%20Music%20genre%20classification:%20Preparing%20the%20dataset/code/extract_data.py

Some Novel Fractional Integral Inequalities for Different Kinds of Convex Functions

Sinan ASLAN[1,2*]

[1] Ağrı Türk Telekom Social Sciences High School, Ağrı Türkiye

[2] Ağrı İbrahim Çeçen University, Institute of Graduate Studies, Ağrı Türkiye

sinanaslan0407@gmail.com (ORCID: 0000-0001-5970-1926)

Abstract

In this paper, some novel integral inequalities for different kinds of convex functions have been proved by using Caputo-Fabrizio fractional integral operators. The findings includes several new integral inequalities $h-$convex functions, $s-$convex functions in the second sense. We have used the properties of Caputo-Fabrizio fractional operator, definitions of different kinds of convex functions and elemantery analysis methods.

Keywords: Caputo-Fabrizio fractional integral operator, $h-$convex functions, $s-$convex functions.

1. Introduction

Inequality theory is a field in which many researchers work, with new findings that can be given applications in many disciplines such as mathematical analysis, statistics, approximation theory and numerical analysis together with convex functions. Although the concept of convex function is a concept intertwined with inequalities by definition, it has also formed the main motivation of many researches with its aesthetic structure, features and different types. Let's start with the definition of this important class of functions.

2. Materials and Methods

Definition 2.1. Let I be on interval in R. Then $f: I \rightarrow R$ is said to be convex, if
$$f(tx + (1-t)y) \leq tf(x) + (1-t)f(y)$$
holds for all $x, y \in I$ and $t \in [0,1]$ (Pečarić et al. 1992).

Definition 2.2. A function $f: R^+ \rightarrow R$, where $R^+ = [0, \infty)$, is said to be $s-$convex in the second sense if
$$f(\alpha x + \beta y) \leq \alpha^s f(x) + \beta^s f(y)$$
for all $x, y \in [0, \infty)$, $\alpha, \beta \geq 0$ with $\alpha + \beta = 1$ and for some fixed $s \in (0,1]$. We denote by K_s^2 the class of all $s-$convex functions (Breckner 1978).

Definition 2.3. (Varosanec 2007) Let $h: J \subseteq R \rightarrow R$ be a non-negative function. We say that $f: I \subseteq R \rightarrow R$ is an $h-$convex function or that f belongs to the class $SX(h, I)$, if f is non-negative and for all $x, y \in I$ and $\alpha \in [0,1]$, we have
$$f(\alpha x + (1-\alpha)y) \leq h(\alpha)f(x) + h(1-\alpha)f(y).$$

Definition 2.4. Let $f \in H^1(0, b), b > a, \alpha \in [0,1]$ then, the definition of the left and right side of Caputo-Fabrizio fractional integral is:
$$\left(^{CF}_a I^\alpha\right)(t) = \frac{1-\alpha}{B(\alpha)}f(t) + \frac{\alpha}{B(\alpha)}\int_a^t f(y)dy,$$
and
$$\left(^{CF}I^\alpha_b\right)(t) = \frac{1-\alpha}{B(\alpha)}f(t) + \frac{\alpha}{B(\alpha)}\int_t^b f(y)dy$$
where $B(\alpha) > 0$ is normalization function (Abdeljawad and Baleanu 2017).

In the sequel of the paper, we will denote normalization function as $B(\alpha)$ with $B(0) = B(1) = 1$.

In (Tariq et al. 2022), the authors provided an integral inequality of Hermite-Hadamard type for preinvex functions via Caputo-Fabrizio fractional integral inequality as follows.

Theorem 2.1. Let $f: I = [k_1, k_1 + \mu(k_2, k_1)] \rightarrow (0, \infty)$ be a preinvex function on $I°$ and $f \in$

$L[k_1, k_1 + \mu(k_2, k_1)]$. If $\alpha \in [0,1]$, then the following inequality holds

$$f\left(\frac{2k_1 + \mu(k_2, k_1)}{2}\right)$$

$$\leq \frac{B(\alpha)}{\alpha\mu(k_2, k_1)}$$

$$\times \left[{}^{CF}_{k_1}I^\alpha\{f(k)\} + {}^{CF}I^\alpha_{k_1+\mu(k_2,k_1)}\{f(k)\}\right.$$

$$\left. - \frac{2(1-\alpha)}{B(\alpha)}f(k)\right]$$

$$\leq \frac{f(k_1) + f(k_2)}{2}$$

where $k \in [k_1, k_1 + \mu(k_2, k_1)]$.

Atangana and Baleanu produced a new derivative operators using Mittag-Leffler function in Caputo-Fabrizio derivative operator as following.

Definition 2.5. (Atangana and Baleanu 2016). Let $f \in H^1(0, b), b > a, \alpha \in [0,1]$ then, the definition of the new fractional derivative is given:

(1.1) $\left({}^{ABC}_aD^\alpha_t\right)[f(t)] =$
$$\frac{B(\alpha)}{1-\alpha}\int_a^t f'(x)E_\alpha\left[-\alpha\frac{(t-x)^\alpha}{(1-\alpha)}\right]dx.$$

Definition 2.6. (Atangana and Baleanu 2016). Let $f \in H^1(0, b), b > a, \alpha \in [0,1]$ then, the definition of the new fractional derivative is given:

(1.2) $\left({}^{ABR}_aD^\alpha_t\right)[f(t)] =$
$$\frac{B(\alpha)}{1-\alpha}\frac{d}{dt}\int_a^t f(x)E_\alpha\left[-\alpha\frac{(t-x)^\alpha}{(1-\alpha)}\right]dx.$$

Equations (1.1) and (1.2) have a non-local kernel. Also in equation (1.1) when the function is constant we get zero.

The related fractional integral operator has been defined by Atangana-Baleanu as follows.

Definition 2.7. The fractional integral associate to the new fractional derivative with non-local kernel of a function $f \in H^1(a, b)$ as defined:

$${}^{AB}_aI^\alpha\{f(t)\} = \frac{1-\alpha}{B(\alpha)}f(t)$$

$$+ \frac{\alpha}{B(\alpha)\Gamma(\alpha)}\int_a^t f(y)(t-y)^{\alpha-1}dy$$

where, $b > a, \alpha \in [0,1]$ (Atangana and Baleanu 2016).

Abdeljawad and Baleanu introduced right hand side of integral operator as following; The right

fractional new integral with ML kernel of order $\alpha \in [0,1]$ is defined by

$${}^{AB}_bI^\alpha\{f(t)\} = \frac{1-\alpha}{B(\alpha)}f(t)$$

$$+ \frac{\alpha}{B(\alpha)\Gamma(\alpha)}\int_t^b f(y)(y-t)^{\alpha-1}dy.$$

where $, b > a, \alpha \in [0,1]$ (Abdeljawad and Baleanu 2017).

For more information related to different kinds of fractional operators, we recommend to the readers the following papers (Abdeljawad 2015, Abdeljawad and Baleanu 2016, Akdemir et al. 2021- Akdemir et al. 2017, Butt et al. 2020, Caputo and Fabrizio 2015- Gürbüz et al. 2020, Rashid et al 2020-Samko et al. 1993, Set 2012, Set et al. 2017).

3. Results

Theorem 3.1. Let $I \subseteq \mathbb{R}$. Suppose that $f: [a, b] \subseteq I \rightarrow \mathbb{R}$ is a $h-$convex function on $[a, b]$ such that $f \in L_1[a, b]$. Then, we have following inequality for Caputo-Fabrizio fractional integrals:

$$\left({}^{CF}_aI^\alpha f\right)(k) + \left({}^{CF}I^\alpha_b f\right)(k)$$

$$\leq \frac{2(1-\alpha)}{B(\alpha)}f(k) + \frac{\alpha(b-a)f(a)}{B(\alpha)}\int_0^1 h(t)\, dt$$

$$+ \frac{\alpha(b-a)f(b)}{B(\alpha)}\int_0^1 h(1-t)\, dt$$

where $B(\alpha) > 0$ is normalization function and $\alpha \in [0,1]$.

Proof. By usining the definition of $h-$convex function, we can write

$$f(ta + (1-t)b) \leq h(t)f(a) + h(1-t)f(b).$$

By integrating both sides of the inequality over $[0,1]$ with respect to t, we get

$$\int_0^1 f(ta + (1-t)b)\, dt$$

$$\leq f(a)\int_0^1 h(t)\, dt$$

$$+ f(b)\int_0^1 h(1-t)\, dt.$$

By changing of the variable as $x = ta + (1-t)b$, we obtain

$$\frac{1}{b-a}\int_a^b f(x)\, dx \leq f(a)\int_0^1 h(t)\, dt$$

$$+ f(b)\int_0^1 h(1-t)\, dt.$$

By multiplying both sides of the above inequality with $\frac{\alpha(b-a)}{B(\alpha)}$ and adding $\frac{2(1-\alpha)}{B(\alpha)}f(k)$, we have

$$\frac{2(1-\alpha)}{B(\alpha)}f(k) + \frac{\alpha}{B(\alpha)}\int_a^b f(x)\,dx$$
$$\leq \frac{2(1-\alpha)}{B(\alpha)}f(k)$$
$$+ \frac{\alpha(b-a)f(a)}{B(\alpha)}\int_0^1 h(t)\,dt$$
$$+ \frac{\alpha(b-a)f(b)}{B(\alpha)}\int_0^1 h(1-t)\,dt.$$

By simplfying the inequality, we get the result

$$\left(\frac{1-\alpha}{B(\alpha)}f(k) + \frac{\alpha}{B(\alpha)}\int_a^k f(x)\,dx\right)$$
$$+ \left(\frac{1-\alpha}{B(\alpha)}f(k) + \frac{\alpha}{B(\alpha)}\int_k^b f(x)\,dx\right)$$
$$\leq \frac{2(1-\alpha)}{B(\alpha)}f(k)$$
$$+ \frac{\alpha(b-a)f(a)}{B(\alpha)}\int_0^1 h(t)\,dt$$
$$+ \frac{\alpha(b-a)f(b)}{B(\alpha)}\int_0^1 h(1-t)\,dt$$

Namely,

$$\left({}^{CF}_a I^\alpha f\right)(k) + \left({}^{CF}I_b^\alpha f\right)(k)$$
$$\leq \frac{2(1-\alpha)}{B(\alpha)}f(k) + \frac{\alpha(b-a)f(a)}{B(\alpha)}\int_0^1 h(t)\,dt$$
$$+ \frac{\alpha(b-a)f(b)}{B(\alpha)}\int_0^1 h(1-t)\,dt.$$

This completes the proof.

Theorem 3.2. Let $I \subseteq \mathbb{R}$. Suppose that $f:[a,b] \subseteq I \rightarrow \mathbb{R}$ is a $s-$convex function in the second sense on $[a,b]$ such taht $f \in L_1[a,b]$. Then, we have the following inequality for Caputo-Fabrizio fractional integrals:
$$\left({}^{CF}_a I^\alpha f\right)(k) + \left({}^{CF}I_b^\alpha f\right)(k)$$
$$\leq \frac{2(1-\alpha)f(k)(s+1) + \alpha(b-a)\big(f(a)+f(b)\big)}{B(\alpha)(s+1)}.$$
where $B(\alpha) > 0$ is normalization function $s \in (0,1]$ and $\alpha \in [0,1]$.

Proof. By usining the definition of $s-$convex function in the second sense, we can write
$$f(ta + (1-t)b) \leq t^s f(a) + (1-t)^s f(b).$$
By integrating both sides of the inequality over $[0,1]$ with respect to t, we get
$$\int_0^1 f(ta+(1-t)b)\,dt$$
$$\leq \int_0^1 t^s f(a)\,dt$$
$$+ \int_0^1 (1-t)^s f(b)\,dt.$$

By changing of the variable as $x = ta + (1-t)b$, and by calculating the right hand side, we obtain
$$\frac{1}{b-a}\int_a^b f(x)\,dx \leq \frac{f(a)+f(b)}{s+1}.$$
By multiplying both sides of the above inequality with $\frac{\alpha(b-a)}{B(\alpha)}$ and adding $\frac{2(1-\alpha)}{B(\alpha)}f(k)$, we have
$$\frac{2(1-\alpha)}{B(\alpha)}f(k) + \frac{\alpha}{B(\alpha)}\int_a^b f(x)\,dx$$
$$\leq \frac{2(1-\alpha)}{B(\alpha)}f(k)$$
$$+ \frac{\alpha(b-a)}{B(\alpha)}\frac{f(a)+f(b)}{s+1}.$$
By simplfying the inequality, we get the result.

$$\left(\frac{1-\alpha}{B(\alpha)}f(k) + \frac{\alpha}{B(\alpha)}\int_a^k f(x)\,dx\right)$$
$$+ \left(\frac{1-\alpha}{B(\alpha)}f(k) + \frac{\alpha}{B(\alpha)}\int_k^b f(x)\,dx\right)$$
$$\leq \frac{2(1-\alpha)}{B(\alpha)}f(k)$$
$$+ \frac{\alpha(b-a)}{B(\alpha)}\frac{f(a)+f(b)}{s+1}$$

Then, it is easy to see

$$\left({}^{CF}_a I^\alpha f\right)(k) + \left({}^{CF}I_b^\alpha f\right)(k)$$
$$\leq \frac{2(1-\alpha)f(k)(s+1) + \alpha(b-a)\big(f(a)+f(b)\big)}{B(\alpha)(s+1)}.$$

This completes the proof

Theorem 3.3. Let $I \subseteq \mathbb{R}$. Suppose that $f:[a,b] \subseteq I \rightarrow \mathbb{R}$ is a $s-$convex function in the second sense on $[a,b]$ such that $f \in L_1[a,b]$. Then, we have the following inequality for Caputo-Fabrizio fractional integrals:
$$\left({}^{CF}_a I^\alpha f\right)(k) + \left({}^{CF}I_b^\alpha f\right)(k)$$
$$\leq \frac{2(1-\alpha)f(k)(ps+1)^{\frac{1}{p}} + \alpha(b-a)\big(f(a)+f(b)\big)}{B(\alpha)(ps+1)^{\frac{1}{p}}}$$
where $B(\alpha) > 0$ is normalization function $s \in (0,1]$, $q > 1, \frac{1}{p} + \frac{1}{q} = 1$ and $\alpha \in [0,1]$.

Proof : By usining the definition of $s-$convex function in the second sense, we can write
$$f(ta + (1-t)b) \leq t^s f(a) + (1-t)^s f(b).$$
By integrating both sides of the inequality over $[0,1]$ with respect to t, we get

$$\int_0^1 f(ta + (1-t)b)\, dt$$

$$\leq f(a) \int_0^1 t^s\, dt$$

$$+ f(b) \int_0^1 (1-t)^s\, dt.$$

If we apply the Hölder's inequality to the right-hand side of the inequality, we get

$$\int_0^1 |f(ta + (1-t)b)|\, dt$$

$$\leq f(a)\left(\left(\int_0^1 t^{ps}\, dt\right)^{\frac{1}{p}} \left(\int_0^1 1^q dt\right)^{\frac{1}{q}}\right)$$

$$+ f(b)\left(\left(\int_0^1 (1-t)^{ps}\, dt\right)^{\frac{1}{p}} \left(\int_0^1 1^q dt\right)^{\frac{1}{q}}\right)$$

$$= f(a)\left(\left(\frac{1}{ps+1}\right)^{\frac{1}{p}} (1^q)^{\frac{1}{q}}\right)$$

$$+ f(b)\left(\left(\frac{1}{ps+1}\right)^{\frac{1}{p}} (1^q)^{\frac{1}{q}}\right).$$

By changing of the variable as $x = ta + (1-t)b$ and by calculating the right hand side, we obtain

$$\frac{1}{b-a}\int_a^b f(x)\, dx \leq \frac{f(a)+f(b)}{(ps+1)^{\frac{1}{p}}}.$$

By multiplying both sides of the above inequality with $\frac{\alpha(b-a)}{B(\alpha)}$ and adding $\frac{2(1-\alpha)}{B(\alpha)} f(k)$, we have

$$\frac{2(1-\alpha)}{B(\alpha)} f(k) + \frac{\alpha}{B(\alpha)}\int_a^b f(x)\, dx$$

$$\leq \frac{2(1-\alpha)}{B(\alpha)} f(k)$$

$$+ \frac{\alpha(b-a)}{B(\alpha)}\frac{f(a)+f(b)}{(ps+1)^{\frac{1}{p}}}.$$

By simplfying the inequality, we get the result

$$\left(\frac{1-\alpha}{B(\alpha)} f(k) + \frac{\alpha}{B(\alpha)}\int_a^k f(x)\, dx\right)$$

$$+ \left(\frac{1-\alpha}{B(\alpha)} f(k) + \frac{\alpha}{B(\alpha)}\int_k^b f(x)\, dx\right)$$

$$\leq \frac{2(1-\alpha)}{B(\alpha)} f(k)$$

$$+ \frac{\alpha(b-a)}{B(\alpha)}\frac{f(a)+f(b)}{(ps+1)^{\frac{1}{p}}}.$$

Then, we can concludethat

$$\left(^{CF}_a I^\alpha f\right)(k) + \left(^{CF} I^\alpha_b f\right)(k)$$

$$\leq \frac{2(1-\alpha)f(k)(ps+1)^{\frac{1}{p}} + \alpha(b-a)\big(f(a)+f(b)\big)}{B(\alpha)(ps+1)^{\frac{1}{p}}}.$$

Theorem 3.4. Let $I \subseteq \mathbb{R}$. Suppose that $f: [a,b] \subseteq I \to \mathbb{R}$ is a $s-$convex function in the second sense on $[a,b]$ such taht $f \in L_1[a,b]$. Then ,we have following inequality for Caputo-Fabrizio fractional integrals:

$$\left(^{CF}_a I^\alpha f\right)(k) + \left(^{CF} I^\alpha_b f\right)(k)$$

$$\leq \frac{2(1-\alpha)}{B(\alpha)} f(k)$$

$$+ \frac{\alpha(b-a)(f(a)+f(b))\big(q + p(ps+1)\big)}{B(\alpha)pq(ps+1)}$$

where $B(\alpha) > 0$ is normalization function $s \in (0,1]$, $q > 1, \frac{1}{p} + \frac{1}{q} = 1$ and $\alpha \in [0,1]$.

Proof : By usining the definition of $s-$convex function in the second sense, we can write

$$f(ta + (1-t)b) \leq t^s f(a) + (1-t)^s f(b).$$

By integrating both sides of the inequality over $[0,1]$ with respect to t, we get

$$\int_0^1 f(ta + (1-t)b)\, dt$$

$$\leq \int_0^1 t^s f(a)\, dt$$

$$+ \int_0^1 (1-t)^s f(b)\, dt.$$

If we apply the Young's inequality to the right-hand side of the inequality, we get

$$\int_0^1 |f(ta + (1-t)b)|\, dt$$

$$\leq f(a)\left(\frac{1}{p}\left(\int_0^1 t^{ps}\, dt\right) + \frac{1}{q}\left(\int_0^1 1^q\, dt\right)\right)$$

$$+ f(b)\left(\frac{1}{p}\left(\int_0^1 (1-t)^{ps}\, dt\right) + \frac{1}{q}\left(\int_0^1 1^q\, dt\right)\right)$$

$$\leq f(a)\left(\frac{1}{p(ps+1)} + \frac{1}{q}\right) + f(b)\left(\frac{1}{p(ps+1)} + \frac{1}{q}\right).$$

By changing of the variable as $x = ta + (1-t)b$ and by calculating the right hand side, we obtain

$$\frac{1}{b-a}\int_a^b f(x)\, dx \leq \frac{(f(a)+f(b))\big(q + p(ps+1)\big)}{pq(ps+1)}.$$

By multiplying both sides of the above inequality with $\frac{\alpha(b-a)}{B(\alpha)}$ and adding $\frac{2(1-\alpha)}{B(\alpha)} f(k)$, we have

$$\frac{2(1-\alpha)}{B(\alpha)}f(k) + \frac{\alpha}{B(\alpha)}\int_a^b f(x)\,dx$$

$$\leq \frac{2(1-\alpha)}{B(\alpha)}f(k)$$

$$+\frac{\alpha(b-a)}{B(\alpha)}\frac{(f(a)+f(b))(q+p(ps+1))}{pq(ps+1)}.$$

By simplfying the inequality, we get the result

$$\left(\frac{1-\alpha}{B(\alpha)}f(k) + \frac{\alpha}{B(\alpha)}\int_a^k f(x)\,dx\right)$$

$$+\left(\frac{1-\alpha}{B(\alpha)}f(k) + \frac{\alpha}{B(\alpha)}\int_k^b f(x)\,dx\right)$$

$$\leq \frac{2(1-\alpha)}{B(\alpha)}f(k)$$

$$+\frac{\alpha(b-a)(f(a)+f(b))(q+p(ps+1))}{B(\alpha)pq(ps+1)}$$

Namely,

$$\left({}_{a}^{CF}I^{\alpha}f\right)(k) + \left({}^{CF}I_b^{\alpha}f\right)(k)$$

$$\leq \frac{2(1-\alpha)}{B(\alpha)}f(k)$$

$$+\frac{\alpha(b-a)(f(a)+f(b))(q+p(ps+1))}{B(\alpha)pq(ps+1)}.$$

Remark 1. If we set $s = 1$ in the main findings, we obtain new estimations for convex functions via Caputo-Fabrizio fractional integrals.

References

ABDELJAWAD, THABET. On conformable fractional calculus. *Journal of computational and Applied Mathematics*, 2015, 279: 57-66.

ABDELJAWAD, THABET; BALEANU, DUMITRU. Integration by parts and its applications of a new nonlocal fractional derivative with Mittag-Leffler nonsingular kernel. *arXiv preprint arXiv:1607.00262*, 2016.

ABDELJAWAD, THABET; BALEANU, DUMITRU. On fractional derivatives with exponential kernel and their discrete versions. *Reports on Mathematical Physics*, 2017, 80.1: 11-27.

AKDEMİR, A. O.; ASLAN, S.; ÇAKALOĞLU, M.N. EKİNCİ, A. Some New Results for Different Kinds of Convex Functions CaputoFabrizio Fractional Operators. 4th International Conference on Mathematical and Related Sciences. Page (92) ICMRS 2021.

AKDEMİR, A. O.; ASLAN, S.; ÇAKALOĞLU, M.N. SET, E. New Hadamard Type Integral Inequalities via Caputo-Fabrizio Fractional Operators. 4th International Conference on Mathematical and Related Sciences. Page (91) ICMRS 2021.

AKDEMİR, A. O.; ASLAN, S.; EKİNCİ, A. Novel Approaches for s-Convex Functions via Caputo-Fabrizio Fractional Integrals. *Proceedings of IAM*, 2022, 11.1: 3-16.

AKDEMIR, AHMET OCAK, et al. New general variants of Chebyshev type inequalities via generalized fractional integral operators. *Mathematics*, 2021, 9.2: 122.

AKDEMIR, AHMET OCAK; EKINCI, ALPER; SET, ERHAN. Conformable fractional integrals and related new integral inequalities. 2017.

ATANGANA, ABDON; BALEANU, DUMITRU. New fractional derivatives with nonlocal and non-singular kernel: theory and application to heat transfer model. *arXiv preprint arXiv:1602.03408*, 2016.

BRECKNER, WOLFGANG W. Stetigkeitsaussagen für eine Klasse verallgemeinerter konvexer Funktionen in topologischen linearen Räumen. *Publ. Inst. Math.(Beograd)(NS)*, 1978, 23.37: 13-20.

BUTT, SAAD IHSAN, et al. New Hermite–Jensen–Mercer-type inequalities via k-fractional integrals. *Advances in Difference Equations*, 2020, 2020: 1-24.

CAPUTO, MICHELE; FABRIZIO, MAURO. A new definition of fractional derivative without singular kernel. *Progress in Fractional Differentiation & Applications*, 2015, 1.2: 73-85.

EKINCI, ALPER; OZDEMIR, MUHAMET. Some new integral inequalities via Riemann-Liouville integral operators. *Applied and computational mathematics*, 2019, 18.3.

GÜRBÜZ, MUSTAFA, et al. Hermite–Hadamard inequality for fractional integrals of Caputo–Fabrizio type and related inequalities. *Journal of Inequalities and Applications*, 2020, 2020: 1-10.

PEAJCARIAAC, JOSIP E.; TONG, YUNG LIANG. *Convex functions, partial orderings, and statistical applications*. Academic Press, 1992.

RASHID, SAIMA, et al. New investigation on the generalized K-fractional integral operators. *Frontiers in Physics*, 2020, 8: 25.

RASHID, SAIMA, et al. New multi-parametrized estimates having pth-order differentiability in fractional calculus for predominating h-convex functions in Hilbert space. *Symmetry*, 2020, 12.2: 222.

SAMKO, STEFAN G., et al. *Fractional integrals and derivatives.* Yverdon-les-Bains, Switzerland: Gordon and breach science publishers, Yverdon, 1993.

SET, ERHAN. New inequalities of Ostrowski type for mappings whose derivatives are s-convex in the second sense via fractional integrals. *Computers & Mathematics with Applications*, 2012, 63.7: 1147-1154.

SET, ERHAN; AKDEMIR, AHMET OCAK; ÖZDEMIR, EMİN. M. Simpson type integral inequalities for convex functions via Riemann-Liouville integrals. *Filomat*, 2017, 31.14: 4415-4420.

TARIQ, MUHAMMAD, et al. New fractional integral inequalities for preinvex functions involving caputo fabrizio operator. 2022.

VAROŠANEC, SANJA. On h-convexity. *Journal of Mathematical Analysis and Applications*, 2007, 326.1: 303-311.

Investigation of Caffeic Acid Effect on Human Cancer Cell Line and Some Enzymes

Lütfi KARAGÖZ[1], Murat ŞENTÜRK[2], Tuğba SAĞIR[3], Yalçin KARAGÖZ[4], Orkun Sanir BATMAZ[5], Muhammet Gürkan KURBAN[5], Fikriye URAS[1]

[1]*Marmara University, Faculty of Pharmacy, Department of Biochemistry, İstanbul, Türkiye*
lutfikaragoz@gmail.com (ORCID: 0000-0002-8183-0350)
furas@marmara.edu.tr (ORCID: 0000-0001-7381-1822)
[2]*Agri Ibrahim Cecen University, Faculty of Pharmacy, Department of Biochemistry, Ağrı, Türkiye*
senturkm36@gmail.com (ORCID: 0000-0002-9638-2896)
[3]*Pim Grup Cosmetics Consultancy, Gokturk, İstanbul, Türkiye*
tubasagir@hotmail.com (ORCID: 0000-0002-3717-8828)
[4]*Agri Ibrahim Cecen University, Faculty of Pharmacy, Department of Pharmaceutical Botany, Ağrı, Türkiye*
ykaragoz@agri.edu.tr (ORCID: 0000-0002-4835-4508)
[5]*Agri Ibrahim Cecen University, Institute of Graduate Studies, Ağrı, Türkiye*
osbatmaz@agri.edu.tr (ORCID: 0009-0006-6682-1241)
gurkan.197430@gmail.com (ORCID: 0009-0003-5309-5293)

Abstract

Caffeic acid, a prominent antioxidant compound, has garnered significant attention in research due to its multifaceted properties, which include anti-inflammatory, antiobesogenic, antithrombotic, vasodilating, and antitumor activities. This study aims to comprehensively investigate the impact of caffeic acid on various metabolic enzymes (carbonic anhydrase I, II, IX, and glutathione reductase) through both *in silico* and *in vitro* approaches. Furthermore, in vitro experiments did conducted on the AGS (gastric cancer cell) line and the HaCaT (keratinocyte normal cell) line to elucidate the effects of caffeic acid in these cellular systems.

Keywords: Caffeic acid, carbonic anhydrase, glutathione reductase, cancer.

1. Introduction

Caffeic acid (CAA) emerges as a polyphenolic entity synthesized via the secondary metabolic pathways occurring within a diverse range of vegetables, notably encompassing olives, coffee beans, fruits, potatoes, carrots, and propolis. Moreover, this constituent assumes a pivotal role as the primary hydroxycinnamic acid derivative prevalent in the human dietary regimen (SILVA et al., 2014; TOSOVIC, 2017).

This phenolic compound (CAA), exists in a range of molecular configurations within the plant kingdom. It is encountered in its elemental state as monomers, taking the form of sugar esters, organic acid esters, glycosides, and amides. Additionally, CAA can adopt more intricate structures, such as dimers, trimers, and flavonoid derivatives. It is also capable of forming associations with proteins and other polymers located in the cellular wall of vegetables (CHEN and HO, 1997; VERMA and HANSCH, 2004; ESPÍNDOLA et al., 2019; SENTURK et al., 2022).

CAA assumes a crucial role in the defense mechanisms deployed by plants to fend off predators, pests, and infections. This compound exhibits inhibitory properties against the proliferation of insects, fungi, and bacteria (TOSOVIC, 2017). Furthermore, it aids in the safeguarding of plant leaves against the harmful effects of ultraviolet

radiation B (UV-B) (GOULD et al., 2000; ESPÍNDOLA et al., 2019; AYGUL et a., 2022).

Extensive investigations, encompassing both *in vitro* and *in vivo* experiments, have substantiated the multifarious physiological effects of CAA and its derivatives. These effects include but are not limited to antibacterial activity (GENARO-MATTOS et al., 2015), anti-inflammatory and antiviral activity (RODRIGUES et al., 2015), cardioprotective and antioxidant activity (AGUNLOYE et al., 2019), antiproliferative and anti-atherosclerotic activity (NAGAOKA et al., 2002; VERMA and HANSCH, 2004), hepatoprotective activity (YANG et al., 2013), anticancer activity (LEE et al.i 2008; MCGLYNN et al., 2015), and anti-hepatocellular carcinoma activity (LEE et al.i 2008; WON et al., 2010). Of particular significance among these properties is the highlighted anti-hepatocarcinoma activity, given the status of hepatocarcinoma (HCC) as a leading cause of cancer-related mortality worldwide (MCGLYNN et al., 2015). Consequently, further exploration concerning the chemical and pharmacological aspects of CAA is imperative to pave the way for potential new drug development and, subsequently, expand therapeutic avenues (ZHANG et al., 2017).

Carbonic anhydrases (CA, EC 4.2.1.1.) play a pivotal role in facilitating the conversion between carbon dioxide (CO_2) and bicarbonate (HCO_3^-) and the subsequent dehydration of bicarbonate, resulting in the regeneration of CO_2 within an acidic milieu (SUPURAN, 2008; FIDAN et al., 2015; YAKAN et al., 2023).

In mammals, a total of sixteen CA isozymes have been identified thus far, with notable emphasis on CA II and CA IX as highly efficient catalysts for carbon dioxide hydration (SUPURAN, 2008; SUPURAN, 2017; ARSLAN et al., 2016; ARSLAN et al., 2020). CA I and II is primarily found in erythrocytes, but also exhibits distribution in numerous secretory tissues of the gastrointestinal tract, kidneys, lungs, eyes, central nervous system, and more. Conversely, CA IX represents a tumor-associated isoform (SUPURAN, 2008; ABDEL-AZIZ et al., 2015; DIZDAROGLU et al., 2020; YAKAN et al., 2023). Moreover, several other CA isoforms have been identified in diverse tissues, actively participating in vital biological processes including acid-base homeostasis, respiration, carbon dioxide and ion transport, bone resorption, ureagenesis,

gluconeogenesis, lipogenesis, and electrolyte secretion. The multitude of CA isozymes involved in these intricate processes hold significant therapeutic potential as they emerge as promising targets for modulation, whether through inhibition or activation, in the treatment of various disorders such as edema, glaucoma, obesity, cancer, and epilepsy (SUPURAN, 2008; SUPURAN, 2017; URCAR et al., 2016; YAKAN et al., 2023).

Glutathione reductase (GR), an enzyme categorized as EC 1.6.4.2, plays a crucial role in maintaining the equilibrium of the intracellular redox system. Its primary function involves facilitating the conversion of oxidized glutathione (GSSG) to reduced glutathione (GSH) through the utilization of nicotinamide adenine dinucleotide phosphate (NADPH) molecules (KARPLUS et al., 1989; COBAN et al., 2007; URCAR et al., 2016). Extensive research has been conducted to explore the inhibition of the GR enzyme using various compounds. The findings of these investigations have consistently indicated a reduction in the GSH/GSSG ratio and an elevation in the $NAD(P)H/NAD(P)^+$ ratio (SENTURK et al., 2008; COUTO et al., 2016; KOCAOGLU et al., 2019; USTUNDAG et al., 2022). Although some studies have demonstrated that GR inhibition does not influence the generation of free radicals or the expression of other enzymes involved in GSH biosynthesis, it is worth noting that the potent activity of the GR enzyme in cancer cells contributes to their resistance against several chemotherapeutic drugs. Increased intracellular GSH levels offer a significant survival advantage for tumor cells, particularly in lung, breast, larynx, colon, and bone marrow cancers. Consequently, the inhibition of the GR enzyme presents a promising avenue for anticancer treatment, considering the potential of such substances (BALENDIRAN et al., 2004; SENTURK et al., 2009; TRAVERSO et al., 2013; SANTACROCE et al., 2023).

In this study, the potential of CAA to inhibit human CA I, II, IX and GR enzymes was tried to be determined. For this purpose, both theoretical (embedding) and experimental experiments were carried out. It also aimed to explore the potential therapeutic effects of CAA on gastric cancer cells and keratinocyte normal cells.

2. Materials and Methods

Chemicals

hCA I (C4396), hCA II (C6165), and hCA IX (CA 9, human recombinant (SRP6483) were procured from Sigma-Aldrich company. All other chemicals and solvents were purchased from Merck (Darmstadt, Germany).

Measurement of Glutathione Reductase Activity

To assess the enzymatic activity of GR, a spectrophotometric method is employed, which involves monitoring the decrease in NADPH levels when the substrate GSSG is present. This reduction in NADPH concentration is measured specifically at a wavelength of 340 nm (BEUTLER, 1984; USTUNDAG et al., 2022).

Measurement of Carbonic Anhydarase Activity

The inhibitory activity of CAA on hCA I, hCA II, and hCA IX were determined according to the esterase method (VERPOORTE et al., 1967; ARSLAN et al. 2020). In inhibitory studies, p-nitrophenyl acetate was employed as the substrate.

Inhibitory Effect Determination of IC$_{50}$ Values of CAA

With inhibitor studies, the activity of CAA, whose solutions were prepared, were added to the cuvette in different concentrations and their activities were measured. CAA were plotted as % Activity- [I], IC$_{50}$ values were calculated from the equation of the curve.

In silico Studies

In silico placement studies were conducted to investigate interactions between CAA and amino acid residues around the active site of the CA I, II, and IX enzyme. All pdb files were obtained from rcsb.org. The AutoDockTools1 program (version 1.5.7) was used for the preparation of all ligands and enzymes. Autodock Vina2 program (version 1.1.2) was used for all docking experiments, the entire surface of each enzyme was investigated, the exhaustiveness value was set as 32, the energy_range value was assigned as 5, and the best 5 results were asked to be listed. Twelve trials of each molecule were made for each enzyme, and the highest scoring conformation of these was aligned with the receptor protein in the PyMOL-oss3 program (version 2.4.1) (SANNER, 1999; TROTT and OLSON, 2010). The evaluation of the interactions was carried out in the Biovia Discovery Studio Visualizer4 (version 21.1.0.2029) program. Docking scores are summarized in Table 1, Figure 2, 3, and 4.

AGS and HaCaT Cell Line Culture Studies

AGS gastric cancer and HaCaT keratinocyte normal cell line attached to the base of the cell culture layer were passaged when their cell density reached 70-80%. Cells were washed with 10 ml of PBS and treated with 4 ml of 0.25% Trypsin/EDTA solution (Gibco) for 2-3 minutes in the incubator to lift them off the flask base and the separation of cells was also observed under the microscope. Trypsin activity was stopped by adding 2 ml of FBS. The cells were then transferred to a 15 ml centrifuge tube and centrifuged at 1800 rpm for 10 minutes at room temperature. The supernatant was completely discarded and the cell pellet was dissolved in 10 ml of DMEM-LG. The mixture was then centrifuged again at 1800 rpm for 10 minutes at room temperature. The supernatant was discarded again, and the cell pellet was dissolved in the appropriate volume of DMEM-LG, and the cells were stained with Trypan blue and counted with a hemocytometer. Depending on the number of cells, cells were seeded into new cell culture dishes in DMEM-LG containing 10% FBS and 0.1 ml/ml Primocin, and the dishes were placed in an incubator at 37°C containing 5% CO$_2$. The MCF-7 cell line was passaged again when they reached 70-80% density (STRIEDINGER et al., 2021).

Cell Viability Test (MTS)

The passaged cells were counted and seeded in two separate 96-well plates with 1x104 cells in each well. After 24 hours of incubation, CAA was given to the cells in the wells at certain concentrations (500, 250, 100, 50, 25 μM). Each concentration was run in 3 replicates. Cell viability test (MTS) was performed after 24 hours. Absorption was measured in the ELISA reader at 450 nm. The graph was drawn according to the resulting absorption values (KOCANCI et al., 2017).

3. Results and Discussion

GR, an antioxidant enzyme, carries out a vital function by regulating the redox metabolism of GSH within the cellular framework of numerous organisms. Its involvement in the modulation of GSH redox hemostasis contributes to the synthesis of deoxyribonucleotides. Moreover, peroxide plays a critical role in the detoxification of 2-oxoaldehydes and xenobiotics. The viability of rapidly dividing cells and those resilient to oxidative stress is significantly reliant on the replenishment of GSH. Consequently, the identification of potential GR inhibitors assumes paramount importance in the advancement of antitumor and antiparasitic pharmaceutical agents (KARPLUS et al., 1989; BOEHME et al., 2000; USTUNDAG et al., 2022).

In investigations concerning the human erythrocyte GR enzyme, which serves as a model for drug trials, it has been ascertained that nitro aromatic compounds containing a quinoline moiety, commonly employed as antisitulant and anticancer medications, exert an influence on the activity of GR enzyme (GRELLIER et al., 2001). Furthermore, diverse substances encompassing certain drugs, metal ions, and nitro groups have been discovered to possess inhibitory properties against GR enzymes derived from various sources (GRELLIER et al., 2001; COBAN et al., 2007; CAKMAK et al., 2011; KOCAOGLU et al., 2019).

In trials for human CA I, II, IX and GR enzymes with CAA. The IC_{50} value for hCA I was determined as 10.26 µM, for hCA II as 9.14 µM, for hCA IX as 8.96 µM and for GR as 25.84 µM. Acetazolamide (AZA) was used as the reference for the tested CA enzymes, and N,N-bis(2-chloroethyl)-N-nitrosourea (BCNU) was used for the GR. AZA was observed as 36.2 µM for hCA I, 0.37 µM for hCA II and 0.93 micromolar for hCA IX. For GR it was observed as 465 µM for BCNU.

The utilization of CA inhibitors in the management of several conditions, such as cancer, glaucoma, and obesity, is well-established. Consequently, the quest for innovative and potent molecular frameworks for the therapeutic intervention of these ailments assumes a noteworthy strategy (ISIK et al., 2015; SUPURAN, 2017; SENTURK et al., 2022).

Three methods were used to determine the solubility of the molecule in water in Swiss-ADME. These are the ESOL, Ali and SILICOS-IT methods. Caffeic acid was estimated to be water soluble according to three methods. In pharmacokinetic estimates, gastrointestinal (GI) absorption was predicted to be high. In the drug similarity part, it shows that the CAA may be active in four of the analyzes of proprietary chemical collections from five different major pharmaceutical companies. According to the estimates of Medicinal Chemistry; It should be used with caution in human therapy as it gives a warning for PAINS (pan assay interference compounds).

Bcolor analysis (to be toxic by default, chemically reactive, metabolically unstable or having properties responsible for poor pharmacokinetics) has given two warnings. In this case, direct use in the body should be well adjusted. There is no similar molecule. Systemic acceptability score is good.
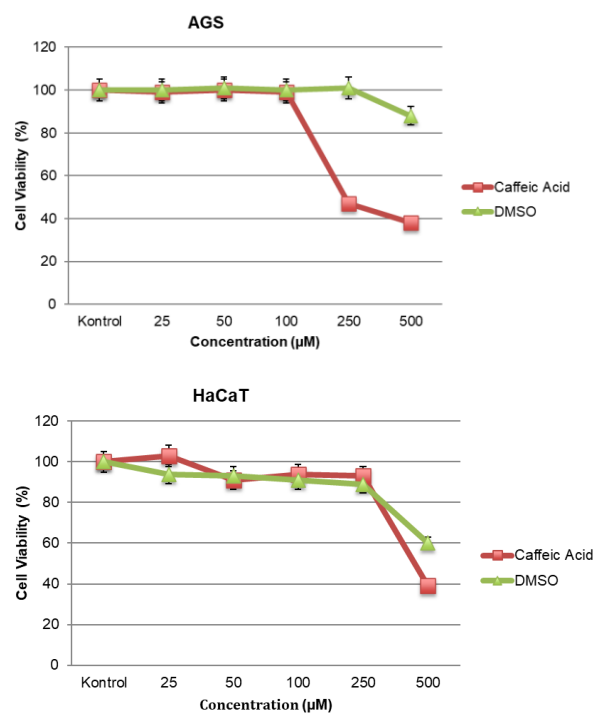
Figure 1. Cell viability result graph of AGS and HaCaT cells treated with 500, 250, 100, 50, 25 µM caffeic acid.

The passaged cells were counted and seeded in two separate 96-well plates with 1×10^4 cells in each well. After 24 hours of incubation, CAA was given to the cells in the wells at certain concentrations (500, 250,

100, 50, 25 µM). Each concentration was run in 3 replicates. Cell viability test (MTS) was performed after 24 hours. Absorption was measured in the ELISA reader at 450 nm. According to the result in Figure 1, in gastric cancer (AGS) cell line, CAA reduced cell viability to 47% and 38%, respectively, at 250 and 500 µM concentrations. As the dose increased, the toxic effect on the gastric cancer cell line also increased. These substances were also tested on a normal human keratinocyte cell line (HaCaT). According to the graph, CAA showed toxic effect only at the highest dose (500 µM), reducing cell viability to 39%.

Using SwissADME, we attempted to calculate physicochemical descriptors as well as predict ADME parameters, pharmacokinetic properties, drug-like nature and medicinal chemistry friendliness of one or more small molecules to support drug discovery (Figure 5).

Table 1. Docking scores and K_i values of caffeic acid for tested enzymes.

Enzyme (PDB ID)	Affinity (kcal/mol)	K_i value (µM)
hCA I (2CAB)	-6,2	5.12
hCA II (3KS3)	-6,5	4.86
hCA IX (6FE2)	-7,2	4.25
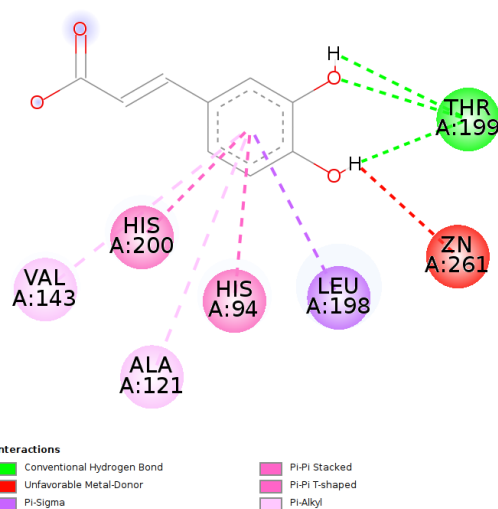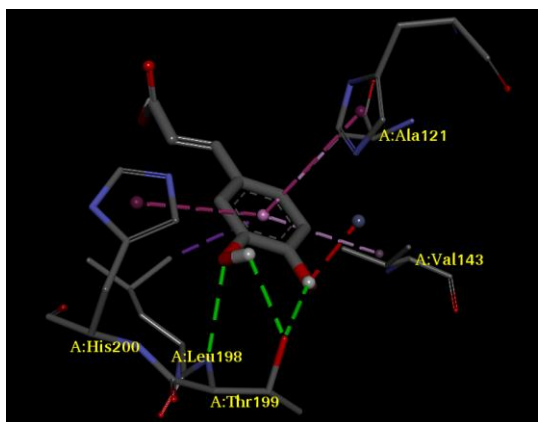
Figure 2. 3D and 2D docking binding models of caffeic acid with hCA I enzyme, respectively.
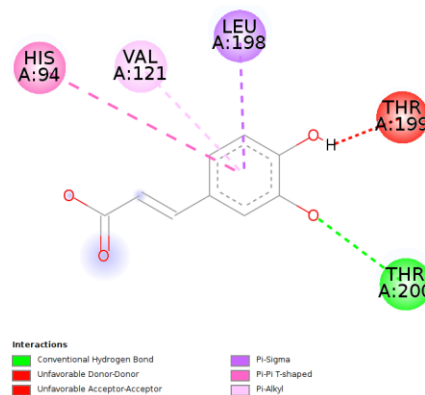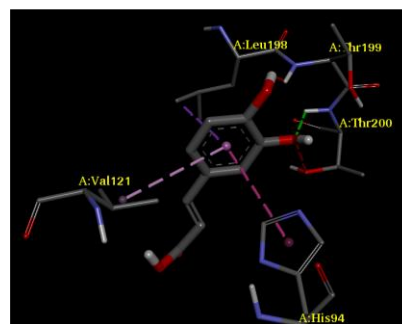
Figure 3. 3D and 2D docking binding models of caffeic acid with hCA II enzyme, respectively.
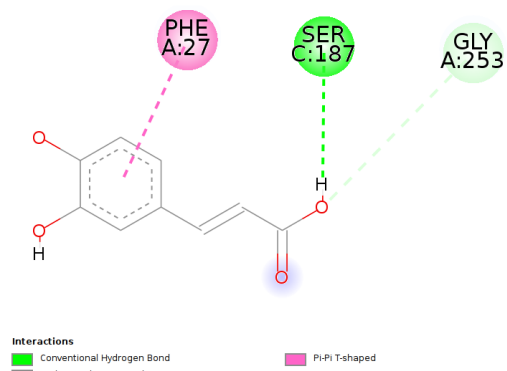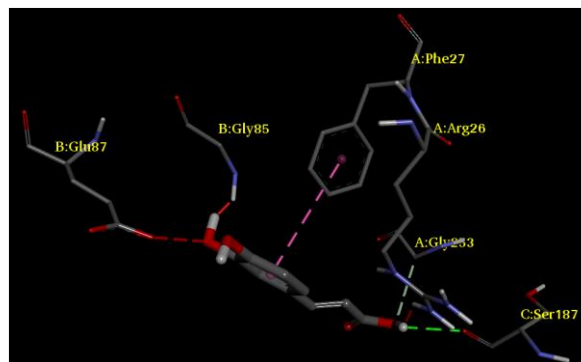
Figure 4. 3D and 2D docking binding models of caffeic acid with hCA IX enzyme, respectively.
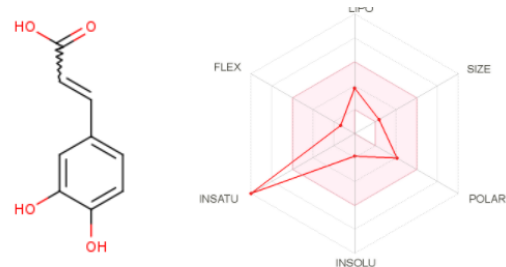
SMILES   OC(=O)/C=C/c1ccc(c(c1)O)O

Physicochemical Properties	
Formula	C9H8O4
Molecular weight	180.16 g/mol
Num. heavy atoms	13
Num. arom. heavy atoms	6
Fraction Csp3	0.00
Num. rotatable bonds	2
Num. H-bond acceptors	4
Num. H-bond donors	3
Molar Refractivity	47.16
TPSA	77.76 Å²
Lipophilicity	
Log $P_{o/w}$ (iLOGP)	0.97
Log $P_{o/w}$ (XLOGP3)	1.15
Log $P_{o/w}$ (WLOGP)	1.09
Log $P_{o/w}$ (MLOGP)	0.70
Log $P_{o/w}$ (SILICOS-IT)	0.75
Consensus Log $P_{o/w}$	0.93
Water Solubility	
Log S (ESOL)	-1.89
Solubility	2.32e+00 mg/ml ; 1.29e-02 mol/l
Class	Very soluble
Log S (Ali)	-2.38
Solubility	7.55e-01 mg/ml ; 4.19e-03 mol/l
Class	Soluble
Log S (SILICOS-IT)	-0.71
Solubility	3.51e+01 mg/ml ; 1.95e-01 mol/l
Class	Soluble
Pharmacokinetics	
GI absorption	High
BBB permeant	No
P-gp substrate	No
CYP1A2 inhibitor	No
CYP2C19 inhibitor	No
CYP2C9 inhibitor	No
CYP2D6 inhibitor	No
CYP3A4 inhibitor	No
Log K_p (skin permeation)	-6.58 cm/s
Druglikeness	
Lipinski	Yes; 0 violation
Ghose	Yes
Veber	Yes
Egan	Yes
Muegge	No; 1 violation: MW<200
Bioavailability Score	0.56
Medicinal Chemistry	
PAINS	1 alert: catechol_A
Brenk	2 alerts: catechol, michael_acceptor_1
Leadlikeness	No; 1 violation: MW<250
Synthetic accessibility	1.81

Figure 5. SwissADME result for caffeic acid.

4. Conclusion

In this investigation, the primary objective is to employ a dual methodology involving in silico and in vitro analyses. The *in silico* assessment will provide valuable insights into the potential interactions of CAA with specific metabolic enzymes. Through this computational approach, the molecular interactions and binding affinities between caffeic acid and target enzymes will be evaluated, offering a preliminary understanding of the possible effects.

Overall, this study seeks to shed light on the in silico and *in vitro* effects of CAA on metabolic enzymes, while simultaneously exploring its potential therapeutic implications in AGS gastric cancer cells and HaCaT keratinocyte normal cells. Through the integration of computational and experimental approaches, this investigation strives to contribute to our understanding of the molecular mechanisms underlying CAA's multifaceted properties and its potential application in cancer therapy.

5. Aknowledgment

References

ABDEL-AZIZ AA-M, EL-AZAB AS, EKINCI D, SENTURK M, SUPURAN CT. 2015. Investigation of arenesulfonyl-2-imidazolidinones as potent carbonic anhydrase inhibitors. J Enzym Inhib Med Chem. 30(1):81-84.

AGUNLOYE OM, OBOH G, ADEMILUYI AO, ADEMOSUN AO, AKINDAHUNSI AA, OYAGBEMI AA, et al. 2019. Cardio-protective and antioxidant properties of caffeic acid and chlorogenic acid: mechanistic role of angiotensin converting enzyme, cholinesterase and arginase activities in cyclosporine induced hypertensive rats. Biomed Pharmacother. 109:450-458.

ARSLAN T, CELIK G, CELIK H, SENTURK M, YAYLI N, EKINCI D. 2016. Synthesis and Biological Evalution of Novel Bischalcone Derivatives as Carbonic Anhydrase Inhibitors. Archive der Pharmazie. 349(9):741-748.

ARSLAN T, TURKOGLU EA, SENTURK M, SUPURAN CT. 2016. Novel chalcone substituted benzenesulfonamides as inhibitors for human carbonic anhydrases. Bioorg Med Chem Lett. 26(24):5867-5870.

ARSLAN T, CEYLAN MB, BAS H, BIYIKLIOGLU Z, SENTURK M. 2020. Design, Synthesis, Characterization of Novel Peripherally Tetra 1,2,3-Triazole Substituted Phthalocyanines and Inhibitor Effect on Cholinesterases (AChE/BChE) and Carbonic Anhydrases (hCA I, II and IX). Dalton Trans. 49:203-209.

AYGUN B, SENTURK M, CINAN E, SIMSEK O, SAYYED MI, KARABULUT A. 2022. Determination of Biological Radioprotective Characteristics of some natural organic compounds for Radiation Shielding Applications. Radiochimica Acta. https://doi.org/10.1515/ract-2022-0028.

BALENDIRAN GK, DABUR R, FRASER D. 2004. The role of glutathione in cancer. Cell Biochem Funct 22:343-352.

BEUTLER E. 1984. Red cell metabolism. A manual of biochemical methods. Grune and Stratton Inc, Orlando. ISBN: 0808916726 9780808916727.

BOEHME CC, ARSCOTT LD, BECKERK, SCHIRMER RH, WILLIAMS CH. 2000. Kinetic characterization of glutathione reductase from the malarial parasite Plasmodium falciparum Comparison with the human enzyme. J Biol Chem. 275:37317-37323.

CAKMAK R, DURDAGI S, EKINCI D, SENTURK M, TOPAL G. 2011. Design, synthesis and biological evaluation of novel nitroaromatic compounds as potent glutathione reductase inhibitors. Bioorg Med Chem Lett. 21;5398-5402.

CHEN JH, HO CT. 1997. Antioxidant activities of caffeic acid and its related hydroxycinnamic

acid compounds. J Agric Food Chem. 45:2374-2378.

COBAN TA, SENTURK M, CIFTCI M, KUFREVIOGLU OI. 2007. Effects of some metal ions on human erythrocyte glutathione reductase: an in vitro study. Protein Peptide Lett. 14(10)1027-1030.

COUTO N, WOOD J, BARBER J. 2016. The role of glutathione reductase and related enzymes on cellular redox homoeostasis network. Free Rad Biol Med. 95:27-42.

DEMIRDAG R, COMAKLI V, SENTURK M, EKINCI D, KUFREVIOGLU OI, SUPURAN CT. 2013. Purification and characterization of carbonic anhydrase from sheep kidney and effects of sulfonamides on enzyme activity. Bioorg Med Chem. 21(6):1522-1525.

DIZDAROGLU Y, ALBAY C, ARSLAN T, ECE A, TURKOGLU EA, EFE A, SENTURK M, SUPURAN CT, EKINCI D. 2020. Design, synthesis and molecular modelling studies of some pyrazole derivatives as carbonic anhydrase inhibitors. J Enzym Inhib Med Chem. 35(1):289-297.

ESPÍNDOLA KMM, FERREIRA RG, NARVAEZ LEM, SILVA ROSARIO ACR, DA SILVA AHM, SILVA AGB, VIEIRA AP, MONTEIRO MC. 2019. Chemical and Pharmacological Aspects of Caffeic Acid and Its Activity in Hepatocarcinoma. Front. Oncol. 9:541.

FIDAN I, SALMAS RE, ARSLAN M, SENTURK M, DURDAGI S, EKINCI D, SENTURK E, COSGUN S. SUPURAN CT. 2015. Carbonic anhydrase inhibitors: design, synthesis, kinetic, docking and molecular dynamics analysis of novel glycine and phenylalanine sulphonamide derivatives. Bioorg Med Chem. 23(23):7353-7358.

GENARO-MATTOS TC, MAURÍCIO ÂQ, RETTORI D, ALONSO A, HERMES-LIMA M. 2015. Antioxidant activity of caffeic acid against iron-induced free radical generation-A chemical approach. PLoS ONE. 10:e0129963.

GOULD KS, MARKHAM KR, SMITH RH, GORIS JJ. 2000. Functional role of anthocyanins in the leaves of Quintinia serrata A. Cunn. J Exp Bot. 51:1107-1115.

GRELLIER P, SARLAUSKAS J, ANUSEVICIUS Z, MAROZIENE A, HOUEE-LEVIN C, SCHREVEL J, CENAS N. 2001. Antiplasmodial activity of nitroaromatic and quinoidal compounds: redox potential vs. inhibition of erythrocyte glutathione reductase. Arch Biochem Biophys. 393:199-206.

ISIK S, VULLO D, DURDAGI S, EKINCI D, SENTURK M, CETIN A, SENTURK E, SUPURAN CT. 2015. Interaction of carbonic anhydrase isozymes I, II, and IX with some pyridine and phenol hydrazinecarbothioamide derivatives. Bioorg Med Chem Lett. 25(23):5636-5641.

KARPLUS PA, PAI EF, SCHULZ GE. 1989. A crystallographic study of the glutathione binding site of glutathione reductase at 0.3 nm resolution. Eur J Biochem. 178:693-703.

KOCANCI FG, HAMAMCIOGLU B, ASLIM B. 2017. The anti-AChE and antiproliferative Activities of Glaucium acutidentatum and Glaucium corniculatum Alkaloid Extracts. J App Pharm Sci. 7(8):191-200.

KOCAOGLU E, TALAZ O, CAVDAR H, SENTURK M, SUPURAN CT, EKINCI D. 2019. Determination of the inhibitory effects of N-methylpyrrole derivatives on glutathione reductase enzyme. J Enzym Inhib Med Chem. 34:51-54.

LEE KW, KANG NJ, KIM JH, LEE KM, LEE DE, HUR HJ, et al. 2008. Caffeic acid phenethyl ester inhibits invasion and expression of matrix metalloproteinase in SK-Hep1 human hepatocellular carcinoma cells by targeting nuclear factor kappa B. Genes Nutr. 2:319-322.

MCGLYNN KA, PETRICK JL, LONDON WT. 2015. Global epidemiology of hepatocellular carcinoma: an emphasis on demographic and regional variability. Clin Liver Dis. 19(2):223-238.

NAGAOKA T, BANSKOTA AH, TEZUKA Y, SAIKI I, KADOTA S. 2002. Selective antiproliferative activity of caffeic acid phenethyl ester analogues on highly liver-Metastatic murine colon 26-L5 carcinoma

cell line. Bioorganic Med Chem. 10:3351-3359.

RODRIGUES JL, ARAÚJO RG, PRATHER KLJ, KLUSKENS LD, RODRIGUES LR. 2015. Heterologous production of caffeic acid from tyrosine in Escherichia coli. Enzyme Microb Technol. 71:36-44.

SANNER MF. 1999. Python: a programming language for software integration and development. J Mol Graph Model. 17(1):57-61.

SANTACROCE G, GENTILE A, SORIANO S, NOVELLI A, LENTI MV, DI SABATINO A. 2023. Glutathione: Pharmacological aspects and implications for clinical use in non-alcoholic fatty liver disease. Front Med (Lausanne). 22;10:1124275.

SENTURK E, GELEN V, SENGUL E, SENTURK M, YILDIRIM S, TEKIN S. 2022. Determination of the Protective Effects of Hesperidin and Curcumin on the Inhibition Effect of 5-Fluorouracil in Mouse Kidney Carbonic Anhydrase Enzyme. Acta Physiol. 234:68.

SENTURK M, KUFREVIOGLU OI, CIFTCI M. 2008. Effects of some antibiotics on human erythrocyte glutathione reductase: An in vitro study, J Enzym Inhib Med Chem. 23(1):144-148.

SENTURK M, KUFREVIOGLU OI, CIFTCI M. 2009. Effects of some analgesic and anestethic drugs on human erythrocyte glutathione reductase: an in vitro study. J Enzym Inhib Med Chem. 24(2):420-424.

SILVA T, OLIVEIRA C, BORGES F. 2014. Caffeic acid derivatives, analogs and applications: a patent review (2009-2013). Expert Opin Ther Pat. 24:1257-1270.

STRIEDINGER K, BARRUET E, POMERANTZ JH. 2021. Purification and preservation of satellite cells from human skeletal muscle. STAR Protoc. 29;2(1):100302.

SUPURAN CT. 2008. Carbonic anhydrases: novel therapeutic applications for inhibitors and activators. Nature Rev Drug Discov. 7:168-181.

SUPURAN CT. 2017. Carbonic anhydrase inhibition and the management of hypotoxic tumours. Metabolites. 7:48-61.

SwissADME: a free web tool to evaluate pharmacokinetics, drug-likeness and medicinal chemistry friendliness of small molecules. Sci Rep. 2017:7:42717.

TOSOVIC J. 2017. Spectroscopic features of caffeic acid: theoretical study. Kragujev J Sci. 3918025435:99-108.

TRAVERSO N, RICCIARELLI R, NITTI M, MARENGO B, FURFARO AL, PRONZATO MA, MARINARI UM, DOMENICOTTI C. 2013. Role of glutathione in cancer progression and chemoresistance. Oxid Med Cell Longev. 2013:972913.

TROTT O, OLSON AJ. 2010. AutoDock Vina: improving the speed and accuracy of docking with a new scoring function, efficient optimization, and multithreading. J Comp chem. 31(2):455-461.

URCAR H, SENTURK E, SENTURK M, GUL M, YILDIRIM S. 2016. Investigation of Effects of Some Catecholamines on The Activity of Carbonic Anhydrase Enzyme Purified From Bovine Kidney Tissue. Acta Physiol. 218:57.

USTUNDAG H, SENTURK E, SENTURK M. 2022. Effect of White Noise and Light Exposure on Rat Testis Glutathione Reductase Enzyme. Acta Physiol. 234:79.

VERMA RP, HANSCH C. 2004. An approach towards the quantitative structure-activity relationships of caffeic acid and its derivatives. ChemBioChem. 5:1188-1195.

VERPOORTE JA, MEHTA S, EDSALL JT. 1967. Esterase activities of human carbonic anhydrases B and C. J Biol Chem. 242(18):4221-4229.

VULLO D., INNOCENTI A., NISHIMORI I., PASTOREK J., SCOZZAFAVA A., PASTOREKOVA S., SUPURAN CT. 2005. Carbonic anhydrase inhibitors. Inhibition of the transmembrane isozyme XII with sulfonamides-a new target for the design of antitumor and antiglaucoma drugs? Bioorg. Med. Chem. Lett. 15:963-969.

WON C, LEE CS, LEE JK, KIM TJ, LEE KH, YANG YM, et al. 2010. CADPE suppresses cyclin D1 expression in hepatocellular

carcinoma by blocking IL-6-induced STAT3 activation. Anticancer Res. 30:481-488.

YAKAN H, BILIR G, ÇAKMAK Ş, TAŞ O, TÜRKÖZ KARAKULLUKÇU N, SOYDAN E, KUTUK H, GUCLU C, SENTURK M, ARSLAN T, OZTURK S, AKSAKAL E, EKINCI D. 2023. Inhibitory effects of sulfenimides on human and bovine carbonic anhydrase enzymes. J Enzyme Inhib Med Chem. 38(1):2194573.

YANG SY, HONG CO, LEE GP, KIM CT, LEE KW. 2013. The hepatoprotection of caffeic acid and rosmarinic acid, major compounds of Perilla frutescens, against t-BHP-induced oxidative liver damage. Food Chem Toxicol. 55:92-99.

ZHANG Z, WANG D, QIAO S, WU X, CAO S, WANG L, ET al. 2017. Metabolic and microbial signatures in rat hepatocellular carcinoma treated with caffeic acid and chlorogenic acid. Sci Rep. 7:4508.

NOTLAR

NOTLAR